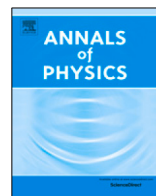




ELSEVIER

Contents lists available at ScienceDirect

Annals of Physics

journal homepage: www.elsevier.com/locate/aop

Local model dynamics for two qubits

Frank Tabakin

Department of Physics and Astronomy, University of Pittsburgh, PA 15260, USA



ARTICLE INFO

Article history:

Received 10 March 2023

Accepted 2 July 2023

Available online 7 July 2023

Keywords:

Quantum simulation

Quantum dynamics

Lindblad equation

Entropy

Density matrix

Qubits

ABSTRACT

The density matrix model described in an earlier paper “Model Dynamics for Quantum Computing” is applied to the case of two qubits. The earlier paper provided a density matrix dynamics with unitary time-dependent gates including qubit energy splitting, entropy constraints, external bath and noise effects. The Lindblad formulation as extended by Beretta was adopted in designing this model. Visualization was provided by examining the time-evolution of the polarization vector. In this paper, the same ideas are applied to two-qubit systems, where there are now 15 time-dependent observables; namely, six polarization vectors (\vec{P}^A, \vec{P}^B), and nine spin-correlations (\vec{T}). These time-dependent observables provide ready visualization of two qubit dynamics. Special emphasis is placed on the CNOT gate, which is implemented following recent outstanding developments in using silicon-based dots. By invoking a different splitting for each qubit, plus a spin-spin interaction and a carefully designed Rabi oscillation, a CNOT gate is generated. Careful analysis of the time-dependence of these aspects provides insight into CNOT dynamics. The model can be used to ascertain the sensitivity and efficacy of such a CNOT gate when subject to external environmental effects such as noise disturbances, and noise compensation, using the single-system formulation of steepest-entropy-ascent (SEA) non-equilibrium quantum thermodynamics, suitable to model controlled-gate implementations as long as the two qubits remain localized and effectively behave as a single physical four-level system. The role of careful timing in constructing an efficient CNOT gate is illustrated. The formation of Bell states and the evolution of entanglement including noise, bath and entropy considerations are examined. Extensions to the two-qubit swap, and to the three-qubit Toffoli gate dynamics are outlined. It is also shown that a simple Lindblad form can be used to introduce weak and distinct qubit noise pulses. A

E-mail address: tabakin@pitt.edu.<https://doi.org/10.1016/j.aop.2023.169408>

0003-4916/© 2023 Elsevier Inc. All rights reserved.

simple scheme for noise compensation is designed to increase purity and decrease entropy, without invocation of quantum correction methodology. It is based on using the preexisting entanglement of the environment with the quantum system and carefully designed non-Hermitian Lindblad pulses.

© 2023 Elsevier Inc. All rights reserved.

1. Introduction

The main goal of this paper is to examine the effect of disturbances on the stability and efficacy of quantum gates as generated by finely-tuned electromagnetic pulses. For that purpose, a density matrix model for a single qubit system was developed in an earlier paper [1]. That paper described time-dependent gates acting on a non-degenerate single qubit. Single qubit NOT and Hadamard gates were incorporated as unitary evolution pulses, which also accounted for the non-degeneracy of the qubit. Noise effects were incorporated using Lindblad operators [2–5] taken as random pulses. The Lindblad form can be used to describe all environmental effects. However, special terms were introduced to isolate and to gain insight into specific environmental effects, such as the bath-system dynamics, and entropy constraints.

The influence of an external bath and entropy dynamics were incorporated by additional Lindblad–Beretta terms, which preserve the Hermiticity, unit trace, and semi-positive properties of the fundamental density matrix. For the entropy aspect, the Beretta form [6–15] is invoked since it includes the idea of steepest-entropy-ascent (SEA) for noiseless open or closed systems. In [14] the dynamics for a single system is developed, which was extended to a composite system in [13]. In this paper, only the single-system formulation is presented, based on the assumption that the double-quantum-dot system is effectively a single physical four-level system which from the point of view of quantum computing may be interpreted as implementing two fully-coupled qubits. The composite-system formulation will be considered in a subsequent study dealing with spatially-separated qubits, for which there is the need to deal with the problems of supraluminal communications (signaling) and non-Hamiltonian energy exchange.

The Beretta et al. description includes definitions of entropy, work, and heat transfer for non-equilibrium systems. Their resultant master equation has many important features, as illustrated in [1]. Indeed, the Lindblad–Beretta master equation has been adopted here as a phenomenological description of quantum computer (QC) dynamics. It includes the essential feature of imposing steepest-entropy-ascent (SEA) for the evolution of a density matrix, which has indeed been elevated to the 4th law for non-equilibrium thermodynamics [6]. As described in Beretta et al. [7] “It is a function of ρ , $\log \rho$ and H designed so as to capture the nonlinear dynamics of an irreversible process by pulling the density or state operator ρ in the direction of the projection of the gradient of the von Neumann entropy functional ...”. Again including supraluminal communications (signaling) is relegated to a future study.

Here the above ideas are applied to the time-evolution of both single and double qubit gates using Hamiltonians that incorporate Rabi oscillations. This replaces our earlier use of a bias pulse to counteract qubit splitting.

The one and two qubit density matrices are discussed in Section 2, where the associated 3 (one qubit) and 15 (two qubit) spin observables are defined. The Hamiltonian that describes qubit non-degeneracy, spin–spin interactions, and the Rabi oscillation is then displayed.

The single qubit case is presented in Appendix A to include generation of NOT and Hadamard gates using Rabi oscillations for a non-degenerate qubit. The detailed dynamics is visualized via the time dependent polarization vector. This update lays the foundation for the extension to two qubits, as presented in Section 3 and in Appendix B. The three-qubit Toffoli gate is presented in Appendix C.

In Section 4, we present the full two qubit model master equation. Several aspects of the model, including an analysis of the Beretta terms are also in Section 4. In Section 5, properties of the full master equation are examined numerically. We use the Mathematica NDSolve for numerical results; alternately, one could invoke Laplace transform and Keldysh [16,17] methods.

Emphasis is on the CNOT gate for open systems, but procedures for setting up swap gates and Bell states are also outlined in Section 5, with emphasis on the role of the CNOT gate on the onset of entanglement.

Distinct weak noise pulses are introduced and their influence examined in Section 5.0.1. A scheme to counter those detrimental noise effects is proposed based on the idea of a curative sequence of weak Lindblad pulses designed to decrease entropy. The initial approach presented here is simply to invoke such pulses to restore lost efficacy. We refer to this as noise compensation (NCO). Error correction methods and/or classical computing information can also be used to complete the noise correction (NC), but that burden is ameliorated somewhat by the initial NCO steps.

In Section 6 conclusions and future plans are discussed.

This work provides a practical dynamic framework for examining, not only the influence of an environment on the efficacy of a QC, but also the loss of reliability in the action of gates and the general loss of coherence. A simple method for partial restoration of stability is proposed.

The master equation designed here incorporates the main features of a density matrix; namely, Hermiticity, unit trace and semi-positive definite character, while also including the evolution of closed and open systems and the effects of gates, noise compensation, noise correction and of an external bath.

2. Density operator for one and two qubits

The density operator [18–20] is an operator in Hilbert space that represents an ensemble of quantum systems. The two-qubit spin density operator, ρ can be understood as a classical ensemble average over a collection of subsystems (the ensemble) which occur in a general state $|\alpha \beta \rangle$, with a joint probability $\mathcal{P}_{\alpha,\beta}$. By a general state, we mean a state of the subsystem that is a general superposition of a complete orthonormal basis (such as eigenstates of a Hamiltonian). For an ensemble of two spin 1/2 particles, $|\alpha \beta \rangle = |\alpha \rangle |\beta \rangle$ is a product of single qubit spinors of the general form

$$\begin{aligned} |\alpha \rangle &= |\hat{n}_\alpha \rangle = \cos(\theta_\alpha/2) e^{-i\phi_\alpha/2} |0\rangle + \sin(\theta_\alpha/2) e^{+i\phi_\alpha/2} |1\rangle \\ |\beta \rangle &= |\hat{n}_\beta \rangle = \cos(\theta_\beta/2) e^{-i\phi_\beta/2} |0\rangle + \sin(\theta_\beta/2) e^{+i\phi_\beta/2} |1\rangle \end{aligned} \tag{1}$$

where the computational basis $|0\rangle$ and $|1\rangle$ denote spin-up and spin-down states, respectively, and α and β label the Euler angles $\theta_\alpha, \phi_\alpha$ and θ_β, ϕ_β , which specify the general directions \hat{n}_α and \hat{n}_β in which qubit A and qubit B are pointing. Writing the spin states in matrix form $|0\rangle \rightarrow \begin{pmatrix} 1 \\ 0 \end{pmatrix}$ and $|1\rangle \rightarrow \begin{pmatrix} 0 \\ 1 \end{pmatrix}$, the above single qubit states are:

$$\begin{aligned} |\alpha \rangle &= \begin{pmatrix} \cos(\theta_\alpha/2) e^{-i\phi_\alpha/2} \\ \sin(\theta_\alpha/2) e^{+i\phi_\alpha/2} \end{pmatrix} \\ |\beta \rangle &= \begin{pmatrix} \cos(\theta_\beta/2) e^{-i\phi_\beta/2} \\ \sin(\theta_\beta/2) e^{+i\phi_\beta/2} \end{pmatrix}. \end{aligned} \tag{2}$$

This general two-qubit state is normalized but not necessarily orthogonal, $\langle \alpha' | \alpha \rangle \neq \delta_{\alpha',\alpha}$ and $\langle \beta' | \beta \rangle \neq \delta_{\beta',\beta}$. The above states are eigenstates of the tensor product operator $(\vec{\sigma} \cdot \hat{n}_\alpha) \otimes (\vec{\sigma} \cdot \hat{n}_\beta)$, where the components of $\vec{\sigma}$ are the Pauli operators.¹

¹ Note: $\vec{\sigma} \cdot \hat{n}_\alpha = \sin \theta_\alpha \cos \phi_\alpha \sigma_1 + \sin \theta_\alpha \sin \phi_\alpha \sigma_2 + \cos \theta_\alpha \sigma_3$.

For a two-qubit system, the definition of a density matrix can be generalized to a product Hilbert space form involving systems of type A and B²

$$\rho_{AB} \equiv \sum_{\alpha, \beta} \mathcal{P}_{\alpha, \beta} |\alpha \beta\rangle \langle \alpha \beta|, \tag{3}$$

where $\mathcal{P}_{\alpha, \beta}$ is the joint probability for finding the two systems with the attributes labeled by α and β . For example, α could designate the possible directions \hat{n}_α of one spin-1/2 system, while β labels the possible spin directions of another spin 1/2 system, \hat{n}_β . One can always ask about the state of just system A or B by summing over or tracing out the other system. For example, the density matrix of system A is picked out of the general definition above by the following partial trace steps³:

$$\begin{aligned} \rho_A &= \text{Tr}_B(\rho_{AB}) \\ &= \sum_{\alpha, \beta} \mathcal{P}_{\alpha, \beta} |\alpha\rangle \langle \alpha| \text{Tr}_B(|\beta\rangle \langle \beta|) \\ &= \sum_{\alpha} \left(\sum_{\beta} \mathcal{P}_{\alpha, \beta} \right) |\alpha\rangle \langle \alpha| \\ &= \sum_{\alpha} \mathcal{P}_{\alpha} |\alpha\rangle \langle \alpha|. \end{aligned} \tag{4}$$

Here the product space is denoted as $|\alpha \beta\rangle \mapsto |\alpha\rangle |\beta\rangle$ and the probability for finding a local state of subsystem A α is defined by

$$\mathcal{P}_{\alpha} = \sum_{\beta} \mathcal{P}_{\alpha, \beta}. \tag{5}$$

This is a standard way to get an individual probability from a joint probability.

It is easy to show that all of the other properties of a one-qubit density matrix still hold true for a composite system case. It has unit trace, it is Hermitian with real eigenvalues and is semi-positive definite.

The quantum rule for the expectation value of a two qubit operator Ω is $\langle \alpha \beta | \Omega | \alpha \beta \rangle$, and for an ensemble of separate quantum subsystems one can form the classical ensemble average $\langle \Omega \rangle$ for the Hermitian observable Ω by taking

$$\langle \Omega \rangle = \frac{\sum_{\alpha \beta} \langle \alpha \beta | \Omega | \alpha \beta \rangle \mathcal{P}_{\alpha \beta}}{\sum_{\alpha \beta} \mathcal{P}_{\alpha \beta}}. \tag{6}$$

The ensemble average is then a simple classical average where $\mathcal{P}_{\alpha \beta}$ is the probability that the particular qubit states $\alpha \beta$ appear in the ensemble. Summing over all possible states of course yields $\sum_{\alpha \beta} \mathcal{P}_{\alpha \beta} = 1$. The above expression is a combination of a classical ensemble average with the quantum mechanical expectation value. It contains the idea that each member of the ensemble interferes only with itself quantum mechanically and that the ensemble involves a simple classical average over the probability distribution of the ensemble.

We now define the two qubit density operator by

$$\rho \equiv \sum_{\alpha \beta} |\alpha \beta\rangle \langle \alpha \beta| \mathcal{P}_{\alpha \beta}. \tag{7}$$

Using closure,⁴ the ensemble average can now be expressed as a ratio of traces

$$\langle \Omega \rangle = \frac{\text{Tr}(\rho \Omega)}{\text{Tr}(\rho)} \equiv \text{Tr}(\rho \Omega), \tag{8}$$

² The sums over α and β can be described as integrals over the associated Euler angles.

³ The property $\text{Tr}_B(|\beta\rangle \langle \beta|) = \langle \beta | \beta \rangle = 1$ is used.

⁴ Closure is a statement that $|n\rangle$ is a complete orthonormal basis and $\sum_n |n\rangle \langle n| = 1$.

which entails the properties

$$\begin{aligned} \text{Tr}(\rho) &= \sum_{m m'} \langle m m' | \rho | m m' \rangle \\ &= \sum_{\alpha \beta} \mathcal{P}_{\alpha \beta} \sum_m \langle \alpha | m \rangle \langle m | \alpha \rangle \sum_{m'} \langle \beta | m' \rangle \langle m' | \beta \rangle \\ &= \sum_{\alpha \beta} \mathcal{P}_{\alpha \beta} \langle \alpha | \alpha \rangle \langle \beta | \beta \rangle = \sum_{\alpha \beta} \mathcal{P}_{\alpha \beta} = 1, \end{aligned} \tag{9}$$

where $|m\rangle$ and $|m'\rangle$ denote complete orthonormal bases (such as the computational basis), and

$$\begin{aligned} \text{Tr}(\rho \Omega) &= \sum_{m \mu m' \mu'} \langle m \mu | \rho | m' \mu' \rangle \langle m' \mu' | \Omega | m \mu \rangle \\ &= \sum_{m \mu m' \mu'} \sum_{\alpha \beta} \mathcal{P}_{\alpha \beta} \langle m \mu | \alpha \beta \rangle \langle \alpha \beta | m' \mu' \rangle \langle m' \mu' | \Omega | m \mu \rangle \\ &= \sum_{\alpha \beta} \mathcal{P}_{\alpha \beta} \langle \alpha \beta | \Omega | \alpha \beta \rangle, \end{aligned} \tag{10}$$

which returns the original ensemble average expression.

The section in Ref. [1] on alternate interpretations of the density matrix can be applied to the present case of two qubits.

2.1. Properties of the density matrix

The definition for two qubits $\rho = \sum_{\alpha \beta} |\alpha \beta\rangle \langle \alpha \beta| \mathcal{P}_{\alpha, \beta}$ is a general one, if we interpret α and β as labels for the locally measurable properties of each qubit. Several important general properties of a density operator follow from this definition. The density operator:

- is Hermitian $\rho^\dagger \equiv \rho$, hence its four eigenvalues are real;
- has unit trace, $\text{Tr}(\rho) \equiv 1$, hence the sum of its four eigenvalues equals 1;
- is semi-positive definite, which means that all of its eigenvalues are greater or equal to zero. This, together with the fact that the density matrix has unit trace, ensures that each density matrix eigenvalue is between zero and one, and yet sum to 1;
- for a pure state, every member of the ensemble has the same quantum state and only one α_0 and one β_0 appear and the density operator becomes $\rho = |\alpha_0 \beta_0\rangle \langle \alpha_0 \beta_0|$. If the state $|\alpha_0 \beta_0\rangle$ is normalized to one then, $\rho^2 = \rho$ and one density matrix eigenvalues is 1, with all others zero;
- for a general ensemble $\rho^2 \leq \rho$ a mixture of possibilities appear as reflected in the probability distribution $\mathcal{P}_{\alpha \beta}$ with the equal sign holding for pure states.

2.2. Classical correlations and entanglement

The density matrix for composite systems can take many forms depending on how the systems are prepared. For example, if distinct systems A & B are independently produced and observed independently, then the density matrix is of product form $\rho_{AB} \mapsto \rho_A \otimes \rho_B$. Then for observables of product form $\Omega_{AB} \mapsto \Omega_A \otimes \Omega_B$, the ensemble average factors

$$\langle \Omega_{AB} \rangle = \frac{\text{Tr}(\rho_{AB} \Omega_{AB})}{\text{Tr}(\rho_{AB})} = \frac{\text{Tr}(\rho_A \Omega_A) \text{Tr}(\rho_B \Omega_B)}{\text{Tr}(\rho_A) \text{Tr}(\rho_B)} = \langle \Omega_A \rangle \langle \Omega_B \rangle, \tag{11}$$

as is expected for two separate uncorrelated spin-spin experiments. For observables of additive form, such as energy for noninteracting subsystems, the ensemble average is a sum of subsystem energies. For such an uncorrelated case, the ensemble average entropy is also a sum of subsystem entropies.

This case can also be expressed as having the joint probability factor $\mathcal{P}_{\alpha, \beta} \mapsto \mathcal{P}_\alpha \mathcal{P}_\beta$ the usual probability rule for uncorrelated systems.

Another possibility for the two systems is that they are prepared in a coordinated manner, with each possible local state of each subsystem assigned a probability based on the correlated preparation technique. For example, consider two colliding beams, A & B, made up of particles with the same spin. Assume the particles are produced in matched pairs with common spin direction \hat{n} . Also assume that the preparation of that pair in that shared direction is produced by design with a classical probability distribution $\mathcal{P}_{\hat{n}}$. Each pair has a density matrix $\rho_{\hat{n}} \otimes \rho_{\hat{n}}$ since they are produced separately, but their spin directions are correlated classically. The density matrix for this case is then

$$\rho_{AB} = \sum_{\hat{n}} \mathcal{P}_{\hat{n}} \rho_{\hat{n}} \otimes \rho_{\hat{n}}. \tag{12}$$

This is a “mixed state” which represents classically correlated preparation and hence any density matrix that can take on the above form can be reproduced by a setup using classically correlated preparations and does *not* represent the essence of Quantum Mechanics, e.g. an entangled state.

An entangled quantum state is described by a density matrix (or by its corresponding state vectors) that is not and cannot be transformed into the two classical forms above; namely, cast into a product or a mixed form. For example, the two-qubit Bell state $\frac{1}{\sqrt{2}}(|01\rangle + |10\rangle)$ has a density matrix

$$\rho = \frac{1}{2}(|01\rangle\langle 01| + |01\rangle\langle 10| + |10\rangle\langle 01| + |10\rangle\langle 10|) \tag{13}$$

that is not of simple product or mixed form. It is the prime example of an entangled state.

2.3. Observables and the density matrix

Visualization of the density matrix and understanding its significance is greatly enhanced by defining associated real spin observables.

2.3.1. One-qubit

The one-qubit density matrix is a 2×2 Hermitian semi-positive definite matrix of unit trace and is fully stipulated by three real parameters. The polarization vector $\vec{P}(t)$, also called the Bloch vector, are the three most useful parameters.

Operators or gates acting on a single qubit state are represented by 2×2 matrices. The dimension of the single qubit state vectors ($|0\rangle$ and $|1\rangle$) is $N = 2^{n_q} = 2$, with $n_q = 1$. The Pauli matrices provide an operator basis of all such matrices. The Pauli-spin matrices are:

$$\sigma_0 = \begin{pmatrix} 1 & 0 \\ 0 & 1 \end{pmatrix}, \sigma_1 = \begin{pmatrix} 0 & 1 \\ 1 & 0 \end{pmatrix}, \sigma_2 = \begin{pmatrix} 0 & -i \\ i & 0 \end{pmatrix}, \sigma_3 = \begin{pmatrix} 1 & 0 \\ 0 & -1 \end{pmatrix}. \tag{14}$$

These are all Hermitian matrices $\sigma_i = \sigma_i^\dagger$. We use the labels (1, 2, 3) to denote the directions (x, y, z). The fourth Pauli matrix σ_0 is simply the 2×2 unit matrix. Any 2×2 matrix can be constructed from these four Pauli matrices, which therefore are an operator basis. That construction applies to the density matrix $\rho(t)$ at any time t. Thus the general form of a one-qubit density matrix, using the four Hermitian Pauli matrices as an operator basis is:

$$\begin{aligned} \rho(t) &= \frac{1}{2} [\sigma_0 + P_1(t) \sigma_1 + P_2(t) \sigma_2 + P_3(t) \sigma_3] \\ &= \frac{1}{2} [\sigma_0 + \vec{P}(t) \cdot \vec{\sigma}] \\ &= \frac{1}{2} \begin{pmatrix} 1 + P_3(t) & P_1(t) - iP_2(t) \\ P_1(t) + iP_2(t) & 1 - P_3(t) \end{pmatrix}, \end{aligned} \tag{15}$$

where the traceless spin operators are $\vec{\sigma} = \{\vec{\sigma}_1, \vec{\sigma}_2, \vec{\sigma}_3\}$, and the real polarization vector is $\vec{P}(t) = \{P_1(t), P_2(t), P_3(t)\}$. The polarization $\vec{P}(t)$ is a real vector, which follows from the Hermiticity of the density matrix $\rho^\dagger(t) \equiv \rho(t)$ and from the ensemble average relation

$$\vec{P}(t) = \text{Tr}(\vec{\sigma} \rho(t)) \equiv \langle \vec{\sigma} \rangle.$$

The above density matrix is clearly Hermitian $\rho^\dagger(t) = \rho(t)$ and of unit trace $\text{Tr}(\rho(t)) = 1$, for real polarization. The semi-positive definite character is assured by the condition $P(t) = |\vec{P}(t)| \leq 1$, i.e. inside the Bloch ball.

Thus specifying the polarization vector (also called the Bloch vector) determines the density matrix and it is convenient to view the polarization as a function of time to gain insight into qubit dynamics.

The semi-positive definite condition for a single qubit follows from determining that the two eigenvalues are $\lambda_1(t) = \frac{1+P(t)}{2}$, $\lambda_2 = \frac{1-P(t)}{2}$, where the length of the polarization vector $P(t) \leq 1$. The unit trace condition becomes simply that the eigenvalues of ρ sum to one

$$\begin{aligned} \text{Tr}(\rho(t)) = 1 &= \text{Tr}(U_\rho(t) \rho_D(t) U_\rho^\dagger(t)) \\ &= \text{Tr}((U_\rho^\dagger(t) U_\rho(t)) \rho_D(t)) \\ &= \text{Tr}(\rho_D(t)) \\ &= \lambda_1(t) + \lambda_2(t), \end{aligned} \tag{16}$$

where $U_\rho(t)$ is the unitary matrix that diagonalizes the density matrix at time t. The diagonal density matrix $\rho_D(t)$ has real eigenvalues along the diagonal. The semi-positive condition now asserts that each of these eigenvalues is greater or equal to zero and less than or equal to one: $0 \leq \lambda_i(t) \leq 1$, while summing to 1. For the one qubit case the above conditions mean that $\lambda_1(t) + \lambda_2(t) = 1$, and since $0 \leq \lambda_i(t) \leq 1$, the length of the polarization vector $P(t)$ remains between zero and one, inside the Bloch ball.

Note that the density matrix, its eigenvalues and associated polarization vector in general depend on time. Indeed, the dynamics of a one-qubit system is best visualized by how the polarization or eigenvalues change in time. The polarization operator is simply $\Omega = \vec{\sigma}$ and we have the following relations for the value and time derivative of the polarization vector:

$$\begin{aligned} \vec{P}(t) &= \text{Tr}(\vec{\sigma} \rho(t)) = \langle \vec{\sigma} \rangle \\ \frac{d\vec{P}(t)}{dt} &= \text{Tr}(\vec{\sigma} \frac{d\rho(t)}{dt}). \end{aligned} \tag{17}$$

2.3.2. Two-qubits

Much of what is presented here applies to multi-qubit and qutrit cases. The main difference for more qubits/qutrits is an increase in the number of polarization and spin correlation observables.

The two-qubit density matrix is a 4×4 Hermitian semi-positive matrix of unit trace and is fully stipulated by 15 real parameters. Note the state vectors are of dimension $N = 2^{n_q} = 4$, with $n_q = 2$ qubits; the density matrix is then a 4×4 matrix, The Hermiticity and trace properties then lead to a count of $2^{n_q} 2^{n_q} - 1 \equiv 15$ parameters. Six of these parameters can be selected to be polarization vectors $\vec{P}^A(t)$ for qubit A and $\vec{P}^B(t)$ for qubit B. The remaining nine parameters are the spin correlations (\overleftrightarrow{T}), written in dyadic form.

More specifically, the two qubit density matrix

$$\begin{aligned} \rho(t) &= \frac{1}{4}(\mathbf{I}_4 + \chi_A^P(t) + \chi_B^P(t) + \chi^T(t)) \\ \chi_A^P(t) &= \sum_{i=1,3} P_i^A(t) \sigma_i^A \otimes \sigma_0^B \\ \chi_B^P(t) &= \sum_{i=1,3} P_i^B(t) \sigma_0^A \otimes \sigma_i^B \\ \chi^T(t) &= \sum_{i,j=1,3} T_{ij}(t) \sigma_i^A \otimes \sigma_j^B \end{aligned} \tag{18}$$

is expressed in terms of the 16 tensor product basis operators $\sigma_i^A \otimes \sigma_j^B$ for $i, j = 0 \dots 3$.

Here $\mathbf{I}_4 \equiv \sigma_0^A \otimes \sigma_0^B$ denotes the 4×4 identity matrix. The $\chi^P(t)$, $\chi^T(t)$ terms are also given below where the Hermitian and traceless aspects are manifest. The polarizations and spin correlations are

Table 1

Density matrix, polarizations and tensor polarizations for some simple cases. The convention used for each qubit is spin up: $\rho = |0\rangle\langle 0|$, spin down : $\rho = |1\rangle\langle 1|$.

ρ	Matrix	\vec{P}^A	\vec{P}^B	$\overleftrightarrow{T}_{AB}$
$ 00\rangle\langle 00 $	$\begin{pmatrix} 1 & 0 & 0 & 0 \\ 0 & 0 & 0 & 0 \\ 0 & 0 & 0 & 0 \\ 0 & 0 & 0 & 0 \end{pmatrix}$	$\{0, 0, 1\}$	$\{0, 0, 1\}$	$\begin{pmatrix} 0 & 0 & 0 \\ 0 & 0 & 0 \\ 0 & 0 & 1 \end{pmatrix}$
$ 01\rangle\langle 01 $	$\begin{pmatrix} 0 & 0 & 0 & 0 \\ 0 & 1 & 0 & 0 \\ 0 & 0 & 0 & 0 \\ 0 & 0 & 0 & 0 \end{pmatrix}$	$\{0, 0, 1\}$	$\{0, 0, -1\}$	$\begin{pmatrix} 0 & 0 & 0 \\ 0 & 0 & 0 \\ 0 & 0 & -1 \end{pmatrix}$
$ 10\rangle\langle 10 $	$\begin{pmatrix} 0 & 0 & 0 & 0 \\ 0 & 0 & 0 & 0 \\ 0 & 0 & 1 & 0 \\ 0 & 0 & 0 & 0 \end{pmatrix}$	$\{0, 0, -1\}$	$\{0, 0, 1\}$	$\begin{pmatrix} 0 & 0 & 0 \\ 0 & 0 & 0 \\ 0 & 0 & -1 \end{pmatrix}$
$ 11\rangle\langle 11 $	$\begin{pmatrix} 0 & 0 & 0 & 0 \\ 0 & 0 & 0 & 0 \\ 0 & 0 & 0 & 0 \\ 0 & 0 & 0 & 1 \end{pmatrix}$	$\{0, 0, -1\}$	$\{0, 0, -1\}$	$\begin{pmatrix} 0 & 0 & 0 \\ 0 & 0 & 0 \\ 0 & 0 & 1 \end{pmatrix}$

now all understood to be time dependent. We use x, y, z to label the $i = 1, 2, 3$ indices.

$$\chi_A^P + \chi_B^P = \begin{pmatrix} P_z^A + P_z^B & P_x^B - iP_y^B & P_x^A - iP_y^A & 0 \\ P_x^B + iP_y^B & P_z^A - P_z^B & 0 & P_x^A - iP_y^A \\ P_x^A + iP_y^A & 0 & -P_z^A + P_z^B & P_x^B - iP_y^B \\ 0 & P_x^A + iP_y^A & P_x^B + iP_y^B & -P_z^A - P_z^B \end{pmatrix}, \tag{19}$$

$$\chi^T(t) = \begin{pmatrix} T_{zz} & T_{zx} - iT_{zy} & T_{xz} - iT_{yz} & T_{xx} - T_{yy} - i(T_{xy} + T_{yx}) \\ T_{zx} + iT_{zy} & -T_{zz} & T_{xx} + T_{yy} + i(T_{xy} - T_{yx}) & -T_{xz} + iT_{yz} \\ T_{xz} + iT_{yz} & T_{xx} + T_{yy} - i(T_{xy} - T_{yx}) & -T_{zz} & -T_{zx} + iT_{zy} \\ T_{xx} - T_{yy} + i(T_{xy} + T_{yx}) & -T_{zx} - iT_{zy} & -T_{xz} - iT_{yz} & T_{zz} \end{pmatrix}.$$

Other 4×4 basis operator sets can be invoked, such as the usual SU(4) representations or a spherical tensor basis; those representations could be useful for displaying interesting dynamical symmetries.⁵

The polarizations and spin correlations are used to monitor the density matrix dynamics. The 15 spin observables are (see Table 1):

$$\{P_x^A, P_y^A, P_z^A\}; \{P_x^B, P_y^B, P_z^B\}; \begin{pmatrix} T_{xx} & T_{xy} & T_{xz} \\ T_{yx} & T_{yy} & T_{yz} \\ T_{zx} & T_{zy} & T_{zz} \end{pmatrix}. \tag{20}$$

Later the effect of exact single NOT and Hadamard gates and of a CNOT gate on the two-qubit spin observables will be stipulated, which will be used to monitor the efficacy of the dynamic pulsed gates. The associated spin observable changes for the production of a Bell state will also be examined.

The relations between the density matrix and the 15 spin observables are:

$$\vec{P}^A(t) = \text{Tr}((\vec{\sigma}_A \otimes \sigma_0) \rho(t)) \equiv \langle \vec{\sigma}_A \otimes \sigma_0 \rangle$$

⁵ The nine spin correlations can be split into scalar S , axial vector \vec{V} , and traceless symmetric τ parts. Here $S = \sum_{i=1,2,3} T_{ii} = \text{Tr}(T)$ and $\vec{V}_x = (T_{yz} - T_{zy})/2$, $\vec{V}_y = (T_{zx} - T_{xz})/2$, $\vec{V}_z = (T_{xy} - T_{yx})/2$. The traceless symmetric part is $\tau_{ij} = (T_{ij} + T_{ji})/2 - \delta_{ij} \text{Tr}(T)/3$. This is the standard decomposition into $1 + 3 + 5$ terms. A decomposition into $J = 0, 1, 2$ spherical tensors terms is another related option.

$$\begin{aligned} \vec{P}^B(t) &= \text{Tr}(\sigma_0 \otimes \vec{\sigma}_B) \rho(t) \equiv \langle \sigma_0 \otimes \vec{\sigma}_B \rangle \\ \overleftrightarrow{T}(t) &= \text{Tr}(\vec{\sigma}_A \otimes \vec{\sigma}_B) \rho(t) \equiv \langle \vec{\sigma}_A \otimes \vec{\sigma}_B \rangle. \end{aligned} \tag{21}$$

The above are used to obtain explicit dynamical equations in terms of the spin observables⁶ using

$$\begin{aligned} \frac{d}{dt} \vec{P}^A(t) &= \text{Tr}(\vec{\sigma}_A \otimes \sigma_0) \frac{d}{dt} \rho(t) \\ \frac{d}{dt} \vec{P}^B(t) &= \text{Tr}(\sigma_0 \otimes \vec{\sigma}_B) \frac{d}{dt} \rho(t) \\ \frac{d}{dt} \overleftrightarrow{T}(t) &= \text{Tr}(\vec{\sigma}_A \otimes \vec{\sigma}_B) \frac{d}{dt} \rho(t). \end{aligned} \tag{22}$$

Note that the partial trace of the above two qubit density matrix yields:

$$\begin{aligned} \text{Tr}_B(\rho(t)) &= \rho^A(t) = \frac{1}{2} \left[\sigma_0 + \vec{P}^A(t) \cdot \vec{\sigma} \right] \\ \text{Tr}_A(\rho(t)) &= \rho^B(t) = \frac{1}{2} \left[\sigma_0 + \vec{P}^B(t) \cdot \vec{\sigma} \right]. \end{aligned} \tag{23}$$

Thus these polarization vectors are subject to the same conditions as for the single qubit case.

Several other quantities are used to monitor the changing state of a quantum system. Later energy, power, heat transfer and temperature concepts will be discussed. First purity, fidelity, and entropy attributes will be examined.

2.3.3. Purity

The purity $\mathcal{P}(t)$ is defined as

$$\mathcal{P}(t) = \langle \rho(t) \rangle = \text{Tr}(\rho(t) \rho(t)) \equiv \sum_{i=1,4} \lambda_i^2. \tag{24}$$

It is called purity since for a pure state density matrix $\rho = |\psi\rangle\langle\psi|$, $\rho^2 = \rho$ and $\text{Tr}(\rho^2) = \text{Tr}(\rho) = 1$, but in general $\text{Tr}(\rho^2) \leq 1$. For a pure state, we see that $\rho^2 = \rho$, implies that each eigenvalue satisfies $\lambda_i(\lambda_i - 1) = 0$, so $\lambda_i = 0$ or 1. Since the eigenvalues sum to 1, a pure state has one eigenvalue equal to one, all others are zero. A mixed or impure state has $\sum_{i=1,2^{nq}} \lambda_i^2 < 1$, which indicates that the nonzero eigenvalues are less than 1.

For a two-qubit system, the purity is simply related to the polarizations and spin correlations

$$\begin{aligned} \mathcal{P}(t) &= \text{Tr}(\rho^2(t)) = \frac{1 + P_A^2(t) + P_B^2(t) + \text{Tr}[\overleftrightarrow{T}^t \overleftrightarrow{T}]}{4}, \\ \dot{\mathcal{P}}(t) &= 2 \text{Tr}(\rho(t) \dot{\rho}(t)) = \frac{1}{2} \left[\vec{P}^A(t) \cdot \frac{d}{dt} \vec{P}^A(t) + \vec{P}^B(t) \cdot \frac{d}{dt} \vec{P}^B(t) \right. \\ &\quad \left. + \text{Tr}[\overleftrightarrow{T}^t \frac{d}{dt} \overleftrightarrow{T}] \right], \end{aligned} \tag{25}$$

where $P_A(t), P_B(t)$ are the lengths of the polarization vectors for qubits A and B. Here \mathbf{T}^t is the transpose of the real 3×3 time-dependent spin correlation matrix:

$$\overleftrightarrow{T} = \begin{pmatrix} T_{11} & T_{12} & T_{13} \\ T_{21} & T_{22} & T_{23} \\ T_{31} & T_{32} & T_{33} \end{pmatrix}.$$

A one-qubit pure state has a polarization vector that is on the unit Bloch ball, whereas its polarization vector is inside the Bloch ball for the impure case. For a two-qubit system, we have $P_A^2(t) + P_B^2(t) + \text{Tr}[\mathbf{T}^t \mathbf{T}] \leq 3$.

⁶ The left arrowheads stress the dyadic aspect of the tensor correlations.

For two uncorrelated qubits $\rho \rightarrow \rho_A \otimes \rho_B$ and $\overleftarrow{T} \rightarrow \overleftarrow{P}_A \overleftarrow{P}_B$, the purity becomes

$$\mathcal{P}(t) = \mathcal{P}_A(t) \mathcal{P}_B(t) = \frac{1 + P_A^2(t)}{2} \frac{1 + P_B^2(t)}{2}.$$

Later we will see how dissipation and entropy dynamics can bring the polarizations inside the Bloch ball and decrease the spin correlations and hence generate impurity.

2.3.4. Fidelity

Fidelity measures the closeness of two states. In its simplest form, this quantity can be defined as $\mathcal{F} = \sqrt{\text{Tr}(\rho_1 \rho_2)}$. For the special case that $\rho_1 = |\psi_1\rangle\langle\psi_1|$ and $\rho_2 = |\psi_2\rangle\langle\psi_2|$, this yields $\mathcal{F} \equiv |\langle\psi_1|\psi_2\rangle|$, which is clearly the magnitude of the overlap probability amplitude.

To align the quantum definition of fidelity with classical probability theory, a more general definition is invoked; namely,

$$\mathcal{F}(\rho_1, \rho_2) \equiv \text{Tr}\left(\sqrt{\sqrt{\rho_1} \rho_2 \sqrt{\rho_1}}\right). \tag{26}$$

When ρ_1 and ρ_2 commute, they can both be diagonalized by the same unitary matrix, but with different eigenvalues. In that limit, we have $\rho_1 = \sum_i \lambda_{1i} |i\rangle\langle i|$ and $\rho_2 = \sum_j \lambda_{2j} |j\rangle\langle j|$ and

$$\mathcal{F}(\rho_1, \rho_2) \equiv \text{Tr}\left(\sqrt{\rho_1 \rho_2}\right) \equiv \sum_i \sqrt{\lambda_{1i} \lambda_{2i}}, \tag{27}$$

which is the classical limit result.

There are additional measures⁷ for the closeness of two states. One of these is the trace distance⁸

$$D_T[\rho_1, \rho_2] = \frac{1}{2} \text{Tr}\left(\sqrt{(\rho_2 - \rho_1)^2}\right),$$

another is the Hilbert–Schmidt distance

$$D_{HS}[\rho_1, \rho_2] = \sqrt{\text{Tr}\left((\rho_2 - \rho_1)^2\right)}.$$

In addition to using the fidelity to monitor the reliability of a CNOT gate, it is convenient to use the Hilbert–Schmidt distance. Comparing a pair of two-qubit density matrices ρ_1 and ρ_2 , the Hilbert–Schmidt distance can be expressed in terms of the differences between the two sets of 15 spin observables as:

$$\begin{aligned} D_{HS}^2[\rho_1, \rho_2] &= D_{HS:P}^2 + D_{HS:T}^2 \tag{28} \\ D_{HS:P}^2 &= \sum_{i=1,3} (P_{1i}^A - P_{2i}^A)^2 + \sum_{i=1,3} (P_{1i}^B - P_{2i}^B)^2 \\ D_{HS:T}^2 &= \sum_{i=1,3} \sum_{j=1,3} (T_{1,ij} - T_{2,ij})^2 \end{aligned}$$

for qubits A and B . Here we see that two density matrices are identical when they have equal spin observables. The above expression for the Hilbert–Schmidt distance squared consists of separate contributions from the qubit A and qubit B polarization vector differences and a last term from the spin correlation differences. The separate terms allows one to identify the main source of density matrix differences.⁹

The fidelity and Hilbert–Schmidt distance will be used to monitor the efficacy or stability of any QC process, where $\rho_1(t)$ is taken as the exact result and $\rho_2(t)$ is the dynamically computed density matrix including Rabi driven gates and decoherence, gate friction, and dissipation effects.

⁷ See [21] for alternate measures of distances between states.

⁸ These measures are equal to zero, rather than one, for equal density matrices.

⁹ The Hilbert–Schmidt distance squared satisfies the relation: $D_{HS}^2[\rho_1, \rho_2] = \text{Tr}(\rho_1^2) + \text{Tr}(\rho_2^2) - 2 \text{Tr}(\rho_1 \rho_2)$.

2.3.5. Entropy

An important property of a quantum state is the entropy. The von Neumann [18] entropy at time t is defined by

$$S(t) = -\text{Tr}(\rho(t) \log_2 \rho(t)). \tag{29}$$

The Hermitian density matrix can be diagonalized by a unitary matrix $U_\rho(t)$ at time t ,

$$\rho(t) = U_\rho(t) \rho^D(t) U_\rho^\dagger(t),$$

where $\rho^D(t)$ is diagonal matrix $\rho^D(t)_{i,j} = \delta_{i,j} \lambda_i$ of the eigenvalues. Then for 2 qubits

$$S(t) = -(\lambda_1 \log_2 \lambda_1 + \lambda_2 \log_2 \lambda_2 + \lambda_3 \log_2 \lambda_3 + \lambda_4 \log_2 \lambda_4). \tag{30}$$

With a base 2 logarithm, the maximum entropy for two qubits is $S_{max} \equiv 2 = n_q$ which occurs when the four eigenvalues are all equal to $1/4$. That case is the most chaotic, or of least information. This occurs when both the polarizations and the spin correlations are zero $\rho = \frac{1}{4} \mathbb{1}_4$.

The minimum entropy of zero obtains when one eigenvalue is one, all others being zero; that is the most organized, maximum information state.

For later use, consider the time derivative of the entropy

$$\begin{aligned} \frac{dS}{dt} &= - \sum_{i=1,4} \left(\frac{d\lambda_i}{dt} \log_2(\lambda_i) + \frac{d\lambda_i}{dt} \right) \\ &= -\text{Tr} \left(\frac{d\rho}{dt} \log_2(\rho(t)) \right). \end{aligned} \tag{31}$$

Since $\text{Tr}(\rho) = \sum_{i=1,4} \lambda_i \equiv 1$, the second rhs term above vanishes.

3. Unitary evolution

A master equation model for the time evolution of a one-qubit density matrix was developed in Ref. [1]. The model included the dynamical evolution under the action of gates and the role of both closed system dynamics and of open system decoherence, dissipation and the system's approach to equilibrium. These aspects are here extended to two-qubits. From the two-qubit density matrix a variety of observables, such as the 15 polarizations and spin correlations, the purity, fidelity, and entropy can be examined as a function of time.

3.1. Unitary evolution

Here we deal with a time-dependent Hamiltonian $H_0 + V(t)$, where the Rabi term is the main source of that time-dependence, but the use of pulses to turn on/off interactions is another. It is well known that time-dependent Hamiltonians yield a unitary time-development operator $U(t, t_0)$. Separating off the static H_0 contribution leads to the Interaction or Dirac picture. The time-dependent term is given by a nested set of multiple time integrals (the Dyson series) with different integration ranges that can be recast as a multiple dimensional set of time integrals with a common t_0, t range, where the series can then be expressed as

$$U(t, t_0) = \mathcal{T} \left(e^{-i \int_{t_0}^t H(\tau) d\tau} \right).$$

Here \mathcal{T} denotes time-ordered. The Magnus method maps this Dyson series into a set of functions that are put into an exponential form which preserves the unitary nature of $U(t, t_0)$ at every level of approximation.

Thus the non-commutativity of $H(t)$ at different times can be incorporated using the Magnus method. When the Magnus method is used for a fine time-grid with infinitesimal time increments dt , the commutator $[H(t), H(t + dt)]$ vanishes and Magnus reduces to only one term. This allows one to simply apply standard nonlinear solution methods, such as the Mathematica code NDSolve

with a fine grid. The fact that NDSolve-based solutions, such as we adopt here, includes the non-commutativity of Hamiltonians at different times has been verified by our numerical studies and noted by Y. Beltukov¹⁰; see [22] for more on this issue. This feature remains true for the Rabi driving terms, the gate pulses and the non-unitary terms as well. For infinitesimal time increments, we then have the unitary evolution or commutator term:

$$\frac{d\rho}{dt} = -\frac{i}{\hbar} [H(t), \rho(t)]. \tag{32}$$

This term specifies the reversible motion of a closed system. To include dissipation, an additional operator \mathcal{L} will be added

$$\dot{\rho} = -\frac{i}{\hbar} [H(t), \rho(t)] + \mathcal{L} \tag{33}$$

which can describe irreversible open or closed systems.

3.2. Hamiltonian

Our Hamiltonian $H(t) = H_0 + V(t)$ is a Hermitian operator in qubit state space; for two qubits it is a 4×4 Hermitian matrix. It consists of a time-independent part $H_0 + V_{SS}$, plus a time-dependent part $V_R(t)$ (see later).

3.2.1. Level splitting

For $n_q = 2$, a typical Hamiltonian H_0 is

$$H_0 \equiv -\frac{1}{2} \hbar \omega_L^A \sigma_z^A \otimes \sigma_0^B - \frac{1}{2} \hbar \omega_L^B \sigma_0^A \otimes \sigma_z^B, \tag{34}$$

which describes a 4 level system shown in Fig. 1 with eigenvalues $-\frac{1}{2} \hbar (\omega_L^A + \omega_L^B)$ for state $|00\rangle$, $-\frac{1}{2} \hbar (\omega_L^A - \omega_L^B)$ for state $|01\rangle$, $+\frac{1}{2} \hbar (\omega_L^A - \omega_L^B)$ for state $|10\rangle$ and $+\frac{1}{2} \hbar (\omega_L^A + \omega_L^B)$ for state $|11\rangle$. We have assumed a common z-direction at this stage for both qubits; the associated magnetic fields are in the same direction but of different magnitudes as reflected in two distinct Larmor frequencies ω_L^A and ω_L^B . This difference can be produced by a magnetic field gradient in the x-y plane.

The polarization vectors for just Hamiltonian H_0 precess about their common \hat{z} direction with the angular frequencies ω_L^A, ω_L^B . This follows from the unitary evolution term

$$\begin{aligned} \frac{d}{dt} \vec{P}^A(t) &= \text{Tr}\left(\left(\vec{\sigma}_A \otimes \sigma_0\right) \frac{d}{dt} \rho(t)\right) = -\frac{i}{\hbar} \text{Tr}\left(\left(\vec{\sigma}_A \otimes \sigma_0\right) [H_0(t), \rho(t)]\right) \\ &= -\frac{i}{\hbar} \text{Tr}\left(\left[\vec{\sigma}_A \otimes \sigma_0, H_0(t)\right] \rho(t)\right) \\ &= +\frac{i}{2} \omega_L^A \text{Tr}_A\left(\left[\vec{\sigma}_A, \sigma_z^A\right] \rho_A(t)\right) \\ &= \vec{\Omega}_L^A \times \vec{P}^A(t) \end{aligned} \tag{35}$$

where $\vec{\Omega}_L^A = \omega_L^A \hat{z}$. The same steps¹¹ hold for qubit B. Thus, the polarization vectors \vec{P}^A and \vec{P}^B precess with their respective Larmor frequencies about the same direction \hat{z} . The polarization vectors then have fixed values of P_z^A and P_z^B and their x and y components vary as

$$P_x^A(t) = P_x^A(0) \cos(\omega_L^A t) + P_y^A(0) \sin(\omega_L^A t) \tag{36}$$

$$P_y^A(t) = P_y^A(0) \cos(\omega_L^A t) - P_x^A(0) \sin(\omega_L^A t)$$

$$P_x^B(t) = P_x^B(0) \cos(\omega_L^B t) + P_y^B(0) \sin(\omega_L^B t) \tag{37}$$

¹⁰ <https://mathematica.stackexchange.com/a/58947/14199>.

¹¹ One step used above is $\text{Tr}(A[B, \rho]) = \text{Tr}([A, B] \rho)$.

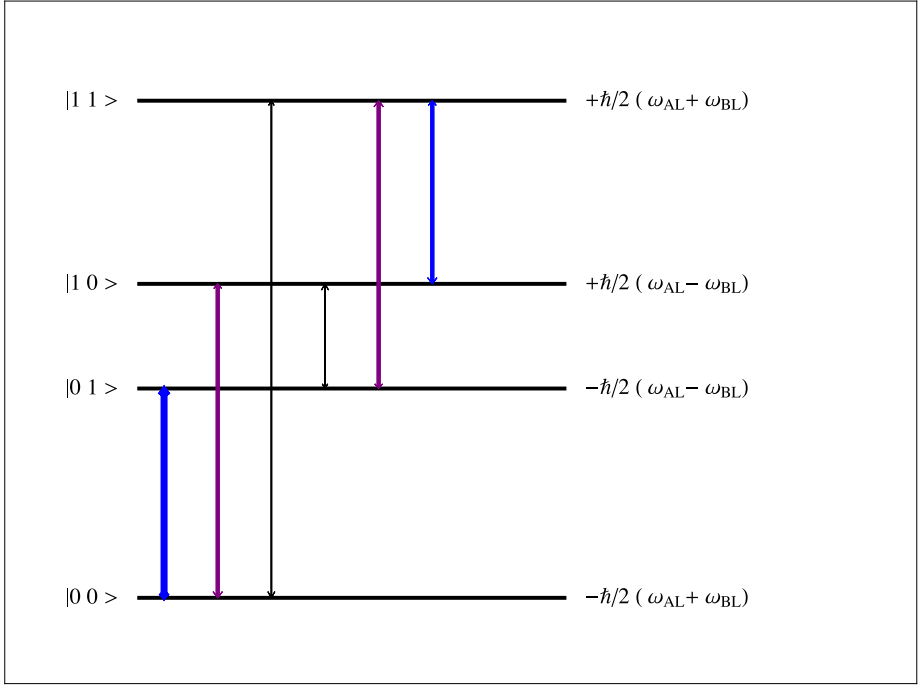


Fig. 1. The two-qubit levels with splittings $\pm \frac{\hbar}{2} (\omega_L^A + \omega_L^B)$, $\pm \frac{\hbar}{2} (\omega_L^A - \omega_L^B)$. We take $\omega_L^A \geq \omega_L^B$. The 6 transitions are indicated by up/down arrows, with the notation Δ_{ab}^{cd} for the $|ab\rangle \leftrightarrow |cd\rangle$ transition. At this stage we have $\Delta_{00}^{01} \equiv \Delta_{10}^{11} \equiv \omega_L^B$, $\Delta_{00}^{10} \equiv \Delta_{01}^{11} \equiv \omega_L^A$, $\Delta_{00}^{11} \equiv \omega_L^A + \omega_L^B$, and $\Delta_{01}^{10} \equiv \omega_L^A - \omega_L^B$. This level scheme will be altered by the spin-spin interaction.

$$P_y^B(t) = P_y^B(0) \cos(\omega_L^B t) - P_x^B(0) \sin(\omega_L^B t)$$

Thus the level splitting $\hbar \omega_L$ produces a precessing polarization with a fixed z-axis value and circular motion in the x-y plane. Next we add a spin-spin interaction to alter the degeneracy of the transition frequencies. This will allow a Rabi oscillation to distinguish between $|00\rangle \leftrightarrow |01\rangle$ versus $|10\rangle \leftrightarrow |11\rangle$ transitions, which is an essential part of obtaining a CNOT gate.

Concerning units, we set \hbar to one and use ω_L to set the frequency and energy scales. For example, using GHz for frequency and $\mu\text{eV} = 10^{-6} \text{ eV}$ for energy, $\hbar = 0.658212 \mu\text{eV}/\text{GHz}$; and we take the energy unit $eu = 0.658212 \mu\text{eV}$. Then $\omega_L = 100 \text{ GHz}$ yields $E = 100 eu$, which is equivalent to using $\hbar = 1$. The time scale of nanoseconds (ns) is associated with $\text{GHz} = 1/\text{ns}$. For the Boltzmann constant we have $\frac{k_B}{\hbar} = 130.92 \text{ GHz}/\text{K}$, independent of energy unit choice. Therefore, $\frac{k_B T}{\hbar} = 130.92 \text{ T (GHz)} \equiv \tau \text{ (GHz)} = \frac{1}{\beta}$, is used in defining both the SEA β_3 and the β_G in the Gibbs density matrix. Other choices based on for example $\hbar = 0.658212 \text{ neV}/\text{MHz}$ can be adopted.

3.2.2. Spin-spin interaction

From Fig. 1, we see that for H_0 alone $\Delta_{00}^{01} \equiv \Delta_{10}^{11} \equiv \omega_L^B$, which means that the same frequency occurs for both transitions. This is not the case for a CNOT gate where the spin B flips only when spin A is 1. Thus it is necessary to produce distinct transition frequencies. Such a difference allows a Rabi spin flip resonance to occur for $|10\rangle \leftrightarrow |11\rangle$ only. To lift the transition degeneracy, we follow Ref. [23–25] and introduce a spin-spin interaction

$$V_{SS}(t) = \frac{J(t)}{4} (\vec{\sigma}_A \cdot \vec{\sigma}_B - \mathbf{I}_4) \tag{38}$$

$$\vec{\sigma}_A \cdot \vec{\sigma}_B = \sum_{i=1,3} \sigma_i^A \otimes \sigma_i^B$$

$$\mathbf{I}_4 = \sigma_0^A \otimes \sigma_0^B,$$

where the \mathbf{I}_4 term is just an overall shift down in the spectrum. This spin–spin interaction is turned on by reducing the potential barrier between the two silicon dots in an experimental tour de force Ref. [23–26]. For degenerate qubits ($\omega_L^A \equiv \omega_L^B$) this shifted spin–spin interaction splits the degenerate $|0 1\rangle$ and $|1 0\rangle$ states into a lower singlet state (by an energy $-\hbar J$), and an unshifted triplet state. For the non-degenerate case, the splitting is a bit more complicated. That case is described by the combinations:

$$|0 1\rangle_c = a_+|0 1\rangle + b_+|1 0\rangle, \tag{39}$$

$$|1 0\rangle_c = a_-|0 1\rangle + b_-|1 0\rangle,$$

$$a_{\pm} = -\frac{\Delta \pm \sqrt{J^2 + \Delta^2}}{\sqrt{2}\sqrt{J^2 + \Delta(\Delta \pm \sqrt{J^2 + \Delta^2})}};$$

$$b_{\pm} = \frac{J}{\sqrt{2}\sqrt{J^2 + \Delta(\Delta \pm \sqrt{J^2 + \Delta^2})}}.$$

with $\Delta = \omega_L^A - \omega_L^B \geq 0$. The eigenvalue of $|0 1\rangle_c$ is $-\frac{1}{2}(J + \sqrt{J^2 + \Delta^2})$; and of $|1 0\rangle_c$ is $-\frac{1}{2}(J - \sqrt{J^2 + \Delta^2})$. In the degenerate limit $\Delta \rightarrow 0$, these eigenvalues reduce to $-J$ for $|0 1\rangle_c \rightarrow$ Singlet state and 0 for $|1 0\rangle_c \rightarrow$ Triplet state. In the no spin–spin limit $J \rightarrow 0$, these eigenvalues reduce to $-(\omega_L^A - \omega_L^B)/2$ for $|0 1\rangle_c \rightarrow |0 1\rangle$ and $+(\omega_L^A - \omega_L^B)/2$ for $|1 0\rangle_c \rightarrow |1 0\rangle$, as seen in Fig. 1. The revised spectrum is illustrated for a fixed value of $J > 0$ in Fig. 2. The new transition frequencies are for example:

$$\delta_{10}^{11} = \frac{\omega_L^A + \omega_L^B}{2} + \frac{1}{2}(J - \sqrt{J^2 + \Delta^2}) \tag{40}$$

$$= \omega_L^B + \frac{J}{2} - \frac{J^2}{4\Delta} \dots$$

$$\delta_{00}^{01} = \frac{\omega_L^A + \omega_L^B}{2} - \frac{1}{2}(J + \sqrt{J^2 + \Delta^2})$$

$$= \omega_L^B - \frac{J}{2} - \frac{J^2}{4\Delta} \dots$$

$$\delta_{01}^{11} = \frac{\omega_L^A + \omega_L^B}{2} + \frac{1}{2}(J + \sqrt{J^2 + \Delta^2})$$

$$= \omega_L^A + \frac{J}{2} + \frac{J^2}{4\Delta} \dots$$

$$\delta_{00}^{10} = \frac{\omega_L^A + \omega_L^B}{2} - \frac{1}{2}(J - \sqrt{J^2 + \Delta^2})$$

$$= \omega_L^A - \frac{J}{2} + \frac{J^2}{4\Delta} \dots$$

With $\Delta > 0, J > 0$, and $J < \Delta$, the series expansion above shows that the magnitude of the δ_{10}^{11} transition frequency is increased, whereas the magnitude of the δ_{00}^{01} transition frequency is decreased from the original ω_L^B value, which provides the required distinction. The need for both spin–spin splitting and level non-degeneracy is apparent here. Note the first two entries above are for the case qubit A is the control qubit and the last two are for when qubit B is the control qubit.

3.2.3. Rabi oscillation

The spectrum in Fig. 2 picks out the essential transition for a dynamical CNOT gate, which is produced using a magnetic field gradient and a spin–spin interaction when the two qubits are

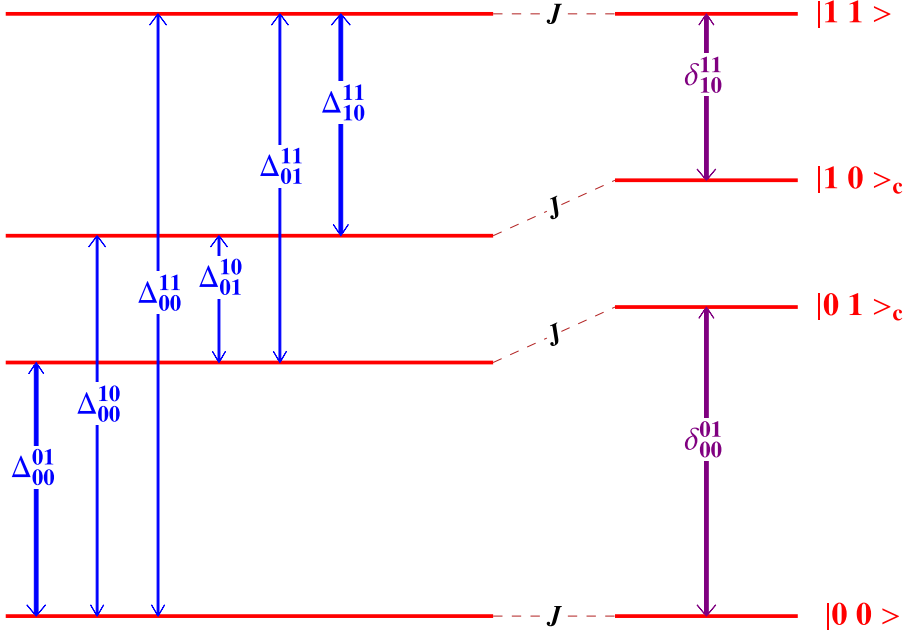


Fig. 2. The two-qubit levels with spin-spin shifts. The transitions are indicated by up/down arrows. The $J = 0$ transitions are denoted by Δ_{ab}^{cd} , and the non-zero J transitions by δ_{ab}^{cd} . The transitions are: $|ab\rangle \leftrightarrow |cd\rangle$. The major difference from the prior level scheme is that δ_{00}^{01} and δ_{10}^{11} are now unequal, which allows a Rabi driving term to cause one type of transition, while having the other minimized as being off-resonance. That is the basic dynamics of a control gate. That example applies for qubit A as the control qubit. For qubit B as the control qubit, δ_{00}^{10} and δ_{01}^{11} are now unequal, which again allows a Rabi driving term to cause one type of transition, while having the other minimized as being off-resonance.

subjected to a Rabi driving interaction in the x-y plane

$$\begin{aligned}
 V_R(t) &= V_R^A(t) + V_R^B(t) \\
 V_R^A(t) &= \frac{\hbar \omega_R^A}{2} (\sigma_x^A \otimes \sigma_0^B \cos(\omega t) - \sigma_y^A \otimes \sigma_0^B \sin(\omega t)) \\
 V_R^B(t) &= \frac{\hbar \omega_R^B}{2} (\sigma_0^A \otimes \sigma_x^B \cos(\omega t) - \sigma_0^A \otimes \sigma_y^B \sin(\omega t)).
 \end{aligned}
 \tag{41}$$

Here ω_R^A and ω_R^B specify the respective strengths of the driving terms and ω denotes the common driving frequency. The two strengths are typically set to a common value $\omega_R^A = \omega_R^B = \omega_2$. The above form describes the effect of an x-y plane rotating B-field, which is selected to yield a NOT gate (σ_x) in the first rotating frame. The Rabi resonance is described in detail in [Appendix A](#), to illustrate its implementation for a simple one-qubit system in preparation for the present two-qubit case.

3.2.4. Two-qubits in first rotating frame

As described in [Appendix B](#), the full two-qubit laboratory frame Hamiltonian $H(t) = H_0 + V_{SS} + V_R(t)$ can now be viewed from a rotating frame using a unitary operator with a common driving frequency ω and strength ω_2 . The new Hamiltonian H_2 is obtained using the procedures described in [Appendices A](#) and [B](#). The two-qubit Hamiltonian in the first rotation frame is:

$$\begin{aligned}
 H_2 &= H_2^A \otimes \sigma_0 + \sigma_0 \otimes H_2^B + V_{SS} \\
 H_2^A &= \vec{\Omega}^A \cdot \vec{\sigma} / 2 \quad \& \quad H_2^B = \vec{\Omega}^B \cdot \vec{\sigma} / 2 \\
 \vec{\Omega}^A &\equiv (\omega - \omega_L^A) \hat{z} + \omega_2^A \hat{x}
 \end{aligned}
 \tag{42}$$

$$\vec{\Omega}^B \equiv (\omega - \omega_L^B)\hat{z} + \omega_2^B \hat{x}.$$

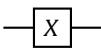
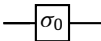
By moving to a rotating frame, the Rabi driving term is here reduced to a simple NOT operator for each qubit, and a shifted z-component strength as incorporated into the vectors $\vec{\Omega}_A, \vec{\Omega}_B$. Since the same rotation is applied to both qubits the spin–spin interaction is the same as in the laboratory frame. The dynamic coupled equations for the 6 polarizations $\vec{P}^A(t), \vec{P}^B(t)$ and the 9 tensor polarizations are presented in Eq. (B.3) of Appendix B.

3.3. Single and control gates

In summary of where we are in setting up two-qubit gates, we have several ingredients as developed in brilliant silicon dot experiments [23,25]. One ingredient is: (1) two distinct non-degenerate qubits, as provided by a z-directed magnetic field with a x–y plane gradient. A second ingredient is: (2) a spin–spin interaction between the qubits, generated by lowering the potential barrier between quantum dots. The third essential ingredient is: (3) a Rabi driving field that is common to both qubits in frequency and strength, as provided by a uniform rotating magnetic field in the x–y plane for a NOT gate and tilted as discussed in Appendix A.2 for a Hadamard gate. How do we combine these ingredients to generate a NOT gate on both qubits or a NOT gate on just one of the qubits? The possible single qubit gates $\Omega_A \otimes \Omega_B$, are itemized by selecting the Ω operators as σ_0, σ_x or as a Hadamard: $(\sigma_z + \sigma_x)/\sqrt{2}$.

3.3.1. Single gates two qubits

First how do we produce the above one and two qubit gates? To produce a NOT gate on qubit A, one should turn off the spin–spin interaction and pick the Rabi frequency ω as ω_L^A . Then qubit B will be off-resonance provided there is a sufficient difference $\omega_L^A - \omega_L^B$, and a suitable strength ω_2 .

The result  is shown later in Fig. 4. This procedure can be repeated for a NOT gate on 

qubit B. For a single qubit Hadamard, a tilted rotated field is used, as discussed in Appendix A.

To get single qubit gates on A and on B, the above steps can be done for A first, then followed by the gate B steps. Alternately, the spin–spin can be zeroed and the two Larmor frequencies set equal and then pairs of single-qubit operators will be established on each of the two qubits.

3.3.2. Control gates

For controlled gates, the spin–spin interaction is essential. It alters the spectrum so that one can select the Rabi frequency ω to pick out $\omega = \delta_{10}^{11}$ (using qubit A as the control) ,

or $\omega = \delta_{11}^{01}$ (using qubit B as the control) .

For suitable non-degeneracies, and splittings, the Rabi driving will have minimal effect on the other transitions. So with all ingredients (1), (2) and (3) on and that choice of ω , we can design the control gate we need. The choice of CNOT or CHAD gate is made by a different orientation of the rotating magnetic field.

3.4. Unitary evolution results

We have clearly followed the lead of the silicon dot community in setting up this case study. It is now necessary to use that setup for the main goal of this paper. That goal is to imbed this dynamics into a Lindblad–Beretta formulation, to test the stability under the demands of entropy, noise and bath effects and to use that dynamics to develop schemes to stabilize the process. Perhaps a set of stabilizing counter pulses can be invoked to ward off evil effects.

Table 2

Typical Parameters for 2 and 3 qubits. For example, CNOT_B denotes the target is B and control qubit is A and Toffoli_B denotes the target is B and control qubits are A & B. The δ_b^a symbols are the Rabi resonance frequencies selected for the associated transitions. The Rabi strength is ω_2 and the spin-spin strength is J.

Name	Symbol	Value
Larmor A	ω_L^A	120
Larmor B	ω_L^B	100
Larmor C	ω_L^C	80
Spin-Spin	J	0.42517
Rabi	ω_2	0.22
CNOT_B	δ_{10}^{11}	100.21
CNOT_A	δ_{01}^{11}	120.215
Toffoli_A	δ_{011}^{111}	120.425
Toffoli_B	δ_{101}^{111}	100.425
Toffoli_C	δ_{110}^{111}	80.425

Table 3

Basic Parameters for \mathcal{L} . Typical strengths for each of the Lindblad functions. The fixed value of (SEA) drives the open system along a path of steepest entropy ascent.

Name	Symbol	Value	Role
\mathcal{L}_1	γ_1	.0	Noise
\mathcal{L}_2	γ_2	.018	Closed
\mathcal{L}_3	γ_3	.018	Open
\dot{S}/\dot{Q}	β_Q	$\frac{1}{120}$	SEA

Table 4

Initial Density Matrix. These define typical single qubit density matrices for qubits A and B. The initial density matrix is then a tensor product $\rho_A \otimes \rho_B$.

Name	Value	Name	Value
p_x^A	-.01	p_x^B	.01
p_y^A	.00	p_y^B	.00
p_x^A	-.99995	p_x^B	-.99995

Table 5

Basic pulse parameters.

Name	Value	Role
t_{on}	6.283	Gate pulse on-time
t_{off}	20.563	Gate pulse off-time
t_f	$4\pi/\gamma_3$	Equilibrium-time SEA
t_f	$2\pi/\omega_2$	Equilibrium final-time
τ_1	.2	Width of gate pulse
τ_2	.2	Width of N pulses
τ_3	.2	Width of NC pulses

3.4.1. Parameters

In Table 2, typical values of $\omega_L^A, \omega_L^B, \omega_2, J$, used in our test cases are shown; these parameters are selected to focus on the role of each term. In Tables 3–5, the typical parameters for \mathcal{L} , for the initial density matrix, and for the pulses are given. Realistic values can be invoked for various experimental conditions.

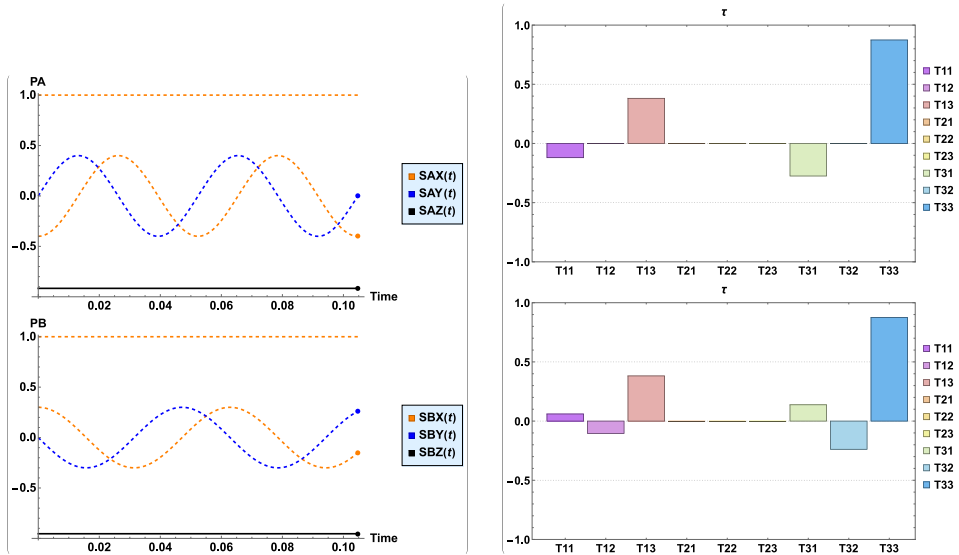


Fig. 3. The 15 spin observables for unitary evolution without gates and no spin-spin interaction. In this case we use the initial values: $P_A = \{-0.4, 0., -0.916\}$, $P_B = \{0.3, 0., -0.954\}$. The top spin-correlations graph is for $t = 0$ and the bottom is for a final time of $2\frac{2\pi}{\omega_L^A} = 0.1047$. That result differs from the initial value since the final polarization vector for qubit B differs from its initial value.

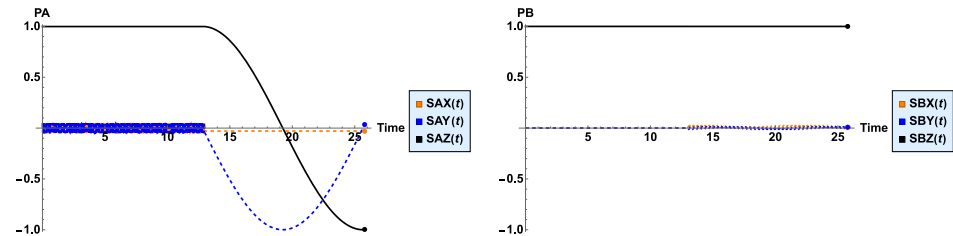


Fig. 4. A single NOT gate acts on qubit A, where the Rabi term is turned on at 12.97 nsec and off at 25.79 s. For qubit A, z-polarization changes from 1 to -1 , the x-polarization remains unchanged and the y-polarization flips, as expected for a NOT gate on qubit A. The case here is $\text{NOT}_A|0, 0\rangle \rightarrow |1, 0\rangle$. Qubit A is on-resonance with $J = 0$ and Rabi resonance $= \omega_L^A = 120$. In contrast, the polarizations for qubit B are off-resonance and are essentially unchanged. Before 12.97 nsec, the figure shows the rapid Larmor precession of the x and y polarizations of qubit A.

3.4.2. No gates

With no gates and zero spin-spin interaction, that is without the Rabi driving term, the system involves simple precession with the two Larmor frequencies ω_L^A, ω_L^B . The six polarization vectors and the nine spin-correlations (tensor polarizations) are shown in Fig. 3. This case is calculated using a pulse to produce the $\omega_L^A > \omega_L^B$ degeneracy. Introducing a spin-spin interaction introduces level splittings as discussed earlier.

3.4.3. NOT gate on qubit A

As discussed earlier, the numerical results for a NOT gate is shown here: Fig. 4.

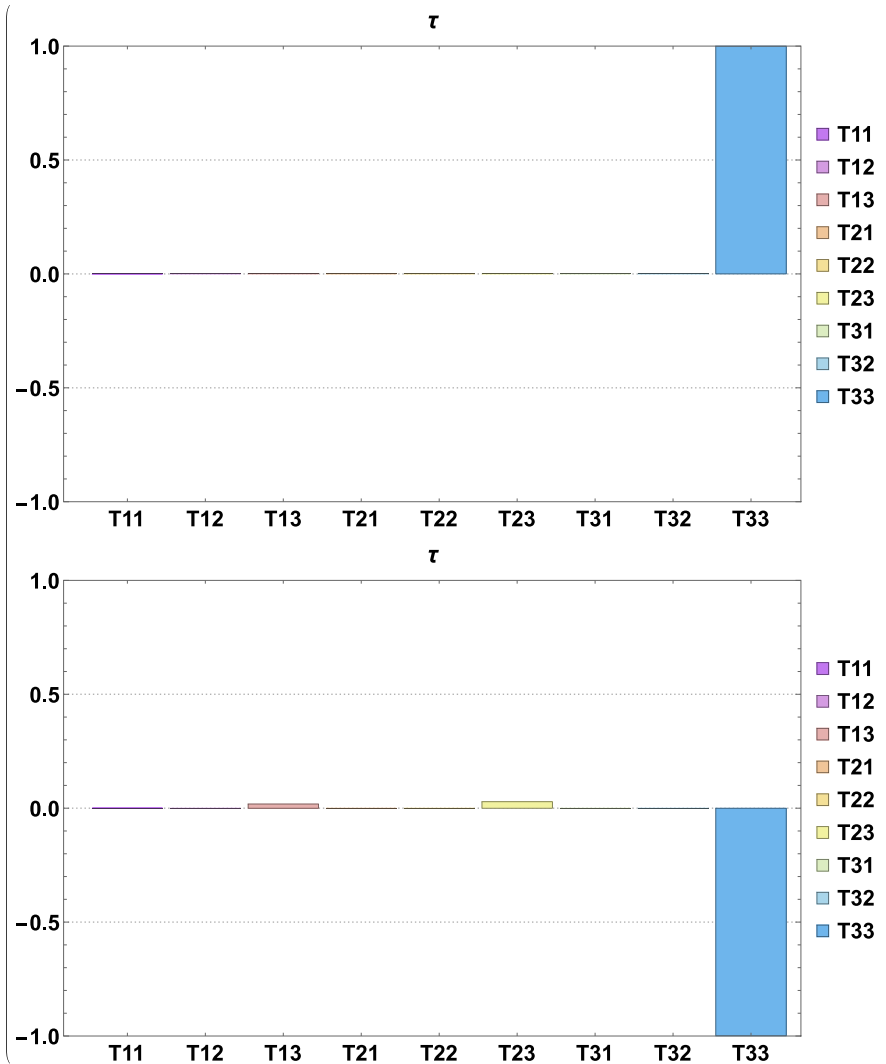


Fig. 6. The nine tensor spin correlations for unitary evolution; e.g., no \mathcal{L} nor noise or noise compensation terms. Initial state case shown is $|11\rangle$ and final state is $|10\rangle$. Top is initial time and bottom is final time. Nonzero values of T_{13} and T_{23} reflect the accuracy of the procedure.

Now we turn on the non-unitary Lindblad terms, including noise which can upset the dynamics and then see how to invoke noise compensation.

4. The model master equation

4.1. Lindblad-Beretta SEA dynamics

The Lindblad-Beretta dynamics discussed in Ref. [1] applies here, except that now the density matrix is of higher dimension 4×4 and there are 15 not just three spin observables. As before the model consists of defining the Lindblad $\mathcal{L}(t)$ operators and how we treat them.

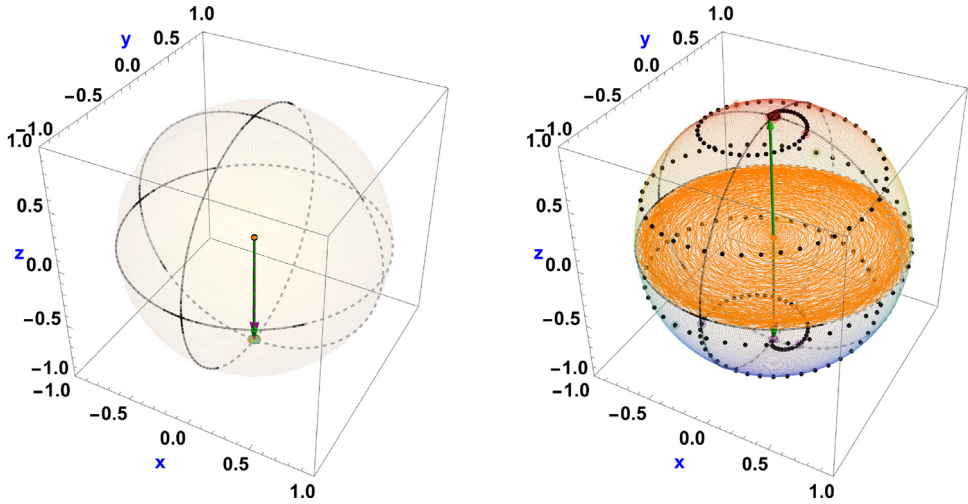


Fig. 7. The polarization vectors for unitary evolution for a CNOTB gate. The left hand side shows the essentially unchanged polarization vector for qubit A. On the right hand side the dotted path shows how the polarization for qubit B changes its direction, with the x-y polarizations projected to the orange x-y plane.

Note that the no-signaling conditions on $\mathcal{L}(t)$ that are required to avoid unphysical supraluminal communications [12–14] have not been included here, but will be in the future.

To the unitary evolution, we now we add a term $\mathcal{L}(t)$ which is required to be Hermitian and traceless so that the density matrix $\rho(t)$ maintains its Hermiticity and trace one properties. In addition, $\mathcal{L}(t)$ has to keep $\rho(t)$ semi-positive definite. To identify explicit physical effects, we separate $\mathcal{L}(t)$ into three terms. Defining “fluctuation” operators by $\hat{H} = H - \langle H \rangle \mathbf{I}_4$ and $\hat{S} = \tilde{S} - \langle \tilde{S} \rangle \mathbf{I}_4$, \mathcal{L}_2 and \mathcal{L}_3 equations simplify for closed systems to:

$$\mathcal{L}_2 = \frac{1}{2} \left\{ \rho(t), \left(\hat{S} - \beta_2(t) \hat{H}(t) \right) \right\}_+, \tag{43}$$

and for open systems to:

$$\mathcal{L}_3 = \frac{1}{2} \left\{ \rho(t), \left(\hat{S} - \beta_3(t) \hat{H}(t) \right) \right\}_+, \tag{44}$$

with $\{A, B\}_+ \equiv AB + BA$ an anti-commutator. Note that $\langle \hat{H} \rangle = 0$ and $\langle \hat{S} \rangle = 0$, where $\langle H \rangle = \text{Tr}(\rho(t)H(t))$ and $\langle \tilde{S} \rangle = \text{Tr}(\rho(t)\tilde{S})$. The operator $\tilde{S} \equiv -\log_e \rho(t)$, involves a base e logarithm to assure that a Gibbs density matrix is obtained in equilibrium.¹³

The level splitting, Rabi and spin-spin interactions and pulses are included in $H(t)$. The state and hence time-dependent functions $\beta_2(t)$, $\beta_3(t)$ will be defined in Eqs. (53) and (58).

The \mathcal{L}_1 is of simplified Lindblad [3] form,

$$\mathcal{L}_1 = \left\{ L(t)\rho(t)L^\dagger(t) - \frac{1}{2}(L^\dagger(t)L(t)\rho(t) + \rho(t)L^\dagger(t)L(t)) \right\}, \tag{45}$$

where the $L(t)$ are time-dependent Lindblad qubit-space operators, which we will represent later as distinct pulses. The most important properties of the $\mathcal{L}_1 \cdots \mathcal{L}_3$ operators are that they are Hermitian and traceless, which means that as the density matrix evolves in time, it remains Hermitian and

¹³ The QC entropy is defined with a base 2 operator $S = -\log_2 \rho(t)$ with entropy equal to $\langle S \rangle = -\text{Tr}(\rho(t) \log_2 \rho(t))$. The conversion factor to base-e is $\tilde{S} \equiv \log_e(2) S$ and $\langle \tilde{S} \rangle \equiv \log_e(2) \langle S \rangle$, with $\log_e(2) = 0.693147$.

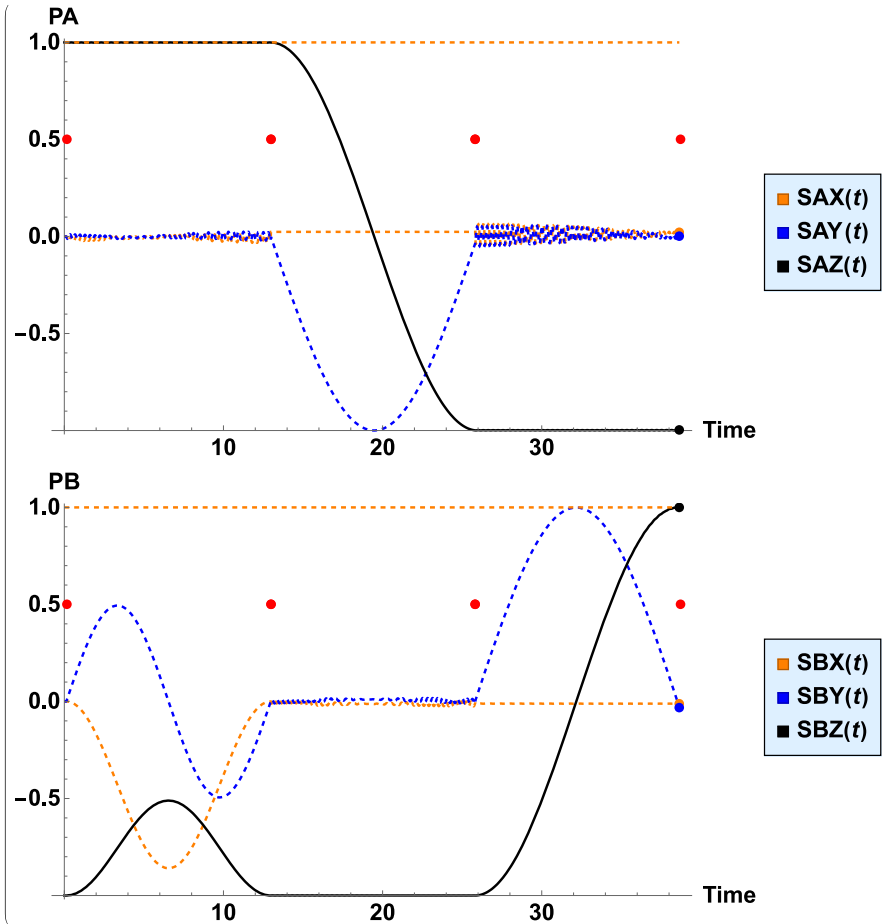


Fig. 8. SW gate spin observables for unitary evolution; e.g., no \mathcal{L} and no noise or noise compensation terms. The red dots indicate the on and off times of each CNOT gate. Initial state is $|01\rangle$ and final state is $|10\rangle$.

of unit trace. They also have the property of maintaining the semi-positive definite property of the density matrix, as proved for $\mathcal{L}_2, \mathcal{L}_3$ by Beretta [8].

The non-unitary terms in the Lindblad–Beretta equation¹⁴ appear as:

$$\mathcal{L} = \gamma_1 \mathcal{L}_1 + \gamma_2 \mathcal{L}_2 + \gamma_3 \mathcal{L}_3, \tag{46}$$

where $\gamma_1, \gamma_2, \gamma_3$ set the rate of each Lindblad term in inverse time units.

In our heuristic master equation, we use the Lindblad form \mathcal{L}_1 to describe the impact of external noise on the system, where we represent the noise as random pulses. In addition, we also use the same Lindblad form to describe dissipative/friction effects on the quantum gates, by having the Lindblad pulses coincide with the action time of the gate pulses. Later this form will be used to introduce noise and also to introduce noise compensation pulses. A strong Lindblad pulse can also represent a quantum measurement.

¹⁴ These definitions will be altered in a future study which will include corrections for unphysical supraluminal effects.

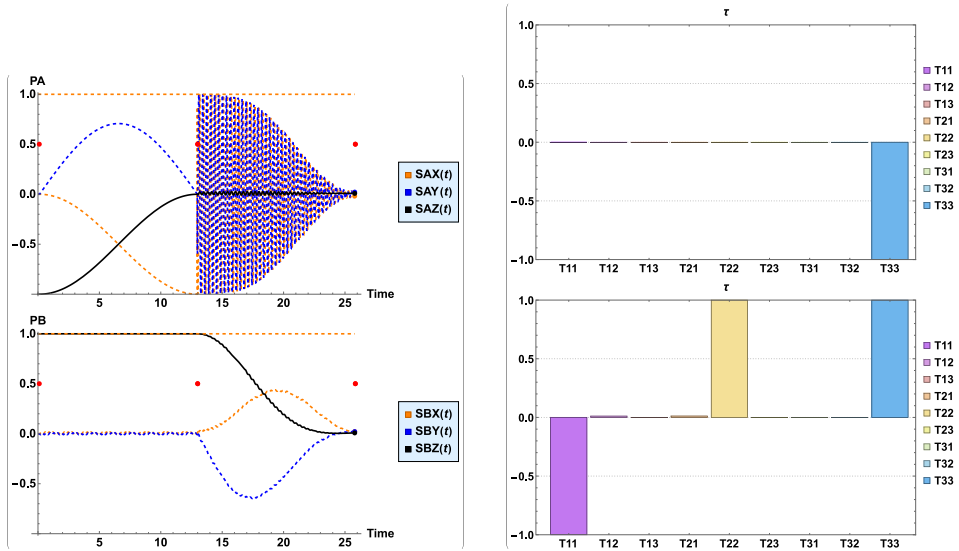


Fig. 9. All 15 Bell gate spin observables for unitary evolution; e.g., no \mathcal{L} nor noise or noise compensation terms. Initial state is $|01\rangle$ and final state is $\frac{1}{\sqrt{2}}(|01\rangle + |10\rangle)$.

The \mathcal{L}_2 term is the Beretta [8] closed system contribution. The closed system involves no heat transfer to an external system, with motion along a path of increasing entropy, as occurs for example with a non-ideal gas in an insulated container. This is accomplished by a state dependent $\beta_2(t)$ that is presented later. Note γ_2 , sets the strength of the Beretta contribution \mathcal{L}_2 , in inverse time units as a fraction of the angular frequency.

A more general \mathcal{L}_3 Bath contribution, based on a general theory [10] of thermodynamics, defines a state dependent $\beta_3(t)$ by using a fixed temperature T_0 to specify a fixed $\dot{Q}(t)/\dot{S}(t)$ ratio (see later). Note γ_3 sets the strength of the \mathcal{L}_3 contribution in inverse time units as a fraction of the angular frequency. This term controls the rate at which an open system achieves equilibrium.

Later, pulsed gates are incorporated into the Hamiltonian $H(t)$ and need to occur well before the \mathcal{L}_3 term becomes important. That is required to avoid the detrimental effects of \mathcal{L}_3 on the gates. In the next section, corrections to certain \mathcal{L} terms due to objectionable supraluminal effects will be addressed, but are not included in this paper.

We seek a simple model that incorporates the main features of qubit dynamics for a quantum computer. These main features include seeing how the dynamics evolve under the action of gates and the role of both closed system dynamics and of open system decoherence, dissipation and the system's approach to equilibrium. From the density matrix we now turn to a variety of observables, all as a function of time.

4.2. SEA and supraluminal effects

The use of the single-system formulation of the Beretta terms \mathcal{L}_2 and \mathcal{L}_3 adopted in the present study is justified when the two-qubit system to be modeled can be assumed to be effectively a single localized physical four-level system. The case of double quantum dots tightly packed in a magnetic field gradient to implement a controlled gate seems to comply with this assumption.

But we emphasize that due to their nonlinearities the single-system Beretta terms are not suitable to model physical implementations in which the experimental setup involves spatially separating and isolating the two qubits from one another. In such cases, the nonlinearities of the single-system SEA terms (and possibly also those of the nonlinear Lindblad terms) would

produce unphysical effects such as energy exchange and correlation buildup even when the two qubits are separated and non-interacting. Such awkward non-local effects include supraluminal communication and are definitely unwanted in proper modeling of composite-system dynamics, but are well-known stumbling blocks to nonlinear extensions of quantum dynamics [27].

When such cases need to be modeled with a proper account of physically acceptable non-local effects, the terms \mathcal{L}_2 and \mathcal{L}_3 should be substituted with the composite-system formulation of steepest-entropy-ascent (SEA) non-equilibrium quantum thermodynamics as already proposed by the original authors [9,10,13]. The author is only at an early stage of examining such formulation, that will be incorporated in future works, also to identify how the Lindblad terms need to be modified to avoid awkward non-local effects.

4.3. Power and heat evolution

The various terms in the master equation play different roles in the dynamics. To examine those differing roles consider the energy of the system and its rate of change. With our Hamiltonian $H(t)$ and a density matrix $\rho(t)$, we form the ensemble average

$$E(t) = \langle H(t) \rangle \equiv \text{Tr}(H(t)\rho(t)).$$

Taking the time derivative, we obtain

$$\begin{aligned} \frac{dE(t)}{dt} &= \text{Tr}\left(\rho(t)\frac{d}{dt}H(t)\right) + \text{Tr}\left(H(t)\frac{d}{dt}\rho(t)\right) \\ &= \frac{d}{dt}W(t) + \frac{d}{dt}Q(t) \end{aligned} \tag{47}$$

$$\dot{W}(t) = \frac{d}{dt}W(t) = \text{Tr}\left(\rho(t)\dot{H}(t)\right)$$

$$\dot{Q}(t) = \frac{d}{dt}Q(t) = \text{Tr}\left(H(t)\dot{\rho}(t)\right) = \text{Tr}\left(\hat{H}(t)\dot{\rho}(t)\right),$$

using $\text{Tr}(\dot{\rho}(t)) = 0$.

We identify the term $\dot{Q}(t)$ as the heat energy transfer rate and $\dot{W}(t)$ as the work per time or power transfer, with the convention that $Q(t) > 0$ indicates heat transferred into the system, and $W(t) > 0$ indicates work done on the system. The time dependence of the density matrix is given by the unitary evolution plus the \mathcal{L} terms of Eq. (43).

Now consider just the power term. Since $\frac{dH(t)}{dt}$ is nonzero when gate pulses are active, power is invoked in the system only via the time derivatives of the gate pulses (and by any undesirable temporal changes in the level splitting).

The energy transfer rate $\dot{Q}(t)$ can now be examined using the dynamic evolution¹⁵

$$\begin{aligned} \text{Tr}\left(\hat{H}(t)\frac{d\rho(t)}{dt}\right) &= \text{Tr}\left[\hat{H}(t)\left\{-\frac{i}{\hbar}[\rho(t), H(t)] + \mathcal{L}\right\}\right] \\ &= \text{Tr}\left(\hat{H}(t)\mathcal{L}\right). \end{aligned} \tag{48}$$

Using the permutation invariance of the trace, the unitary evolution part does not contribute to heat energy transfer. Heat arises from the \mathcal{L} terms. We will now see: (1) how the closed system \mathcal{L}_2 does not generate energy transfer between the overall four level system and its environment, but it does generate energy transfer between the two component qubit subsystems; it does increase entropy; and (2) the open system \mathcal{L}_3 does involve heat. We defer all discussion of the \mathcal{L}_1 Lindblad term until we introduce noise effects.

The heat transfer equation for the closed case is:

$$\dot{Q}(t) = \gamma_2 \left(\langle \hat{H}(t)\hat{S} \rangle - \beta_2(t)\langle \hat{H}(t)\hat{H}(t) \rangle \right) \tag{49}$$

¹⁵ Here the earlier version without correction for signaling is used.

and for the open case is:

$$\dot{Q}(t) = \gamma_3 \left(\langle \hat{H}(t) \hat{S} \rangle - \beta_3(t) \langle \hat{H}(t) \hat{H}(t) \rangle \right), \tag{50}$$

with $\tilde{S} \equiv -\log_e \rho(t)$.

We have:

$$\begin{aligned} \langle H(t) \rangle &\equiv \text{Tr}(\rho(t)H(t)) \\ \langle H(t)H(t) \rangle &\equiv \text{Tr}(\rho(t)H(t)H(t)) \\ \langle \tilde{S} \rangle &\equiv \text{Tr}(\rho(t)\tilde{S}) \\ \langle \tilde{S}\tilde{S} \rangle &\equiv \text{Tr}(\rho(t)\tilde{S}\tilde{S}) \\ \langle H(t)\tilde{S} \rangle &\equiv \text{Tr}(\rho(t)H(t)\tilde{S}) \end{aligned} \tag{51}$$

and

$$\begin{aligned} \langle \hat{H}\hat{H} \rangle &\equiv \langle H(t)H(t) \rangle - \langle H(t) \rangle^2 \\ \langle \hat{H}\hat{S} \rangle &\equiv \langle H(t)\tilde{S} \rangle - \langle H(t) \rangle \langle \tilde{S} \rangle \\ \langle \hat{S}\hat{S} \rangle &\equiv \langle \tilde{S}\tilde{S} \rangle - \langle \tilde{S} \rangle \langle \tilde{S} \rangle, \end{aligned} \tag{52}$$

where the dependence of $\langle \tilde{S} \rangle$ on time is implicit.¹⁶ In the closed case no heat is transferred by fiat and we use $\dot{Q}(t) \equiv 0$ to define $\beta_2(t)$. The major feature of Beretta's \mathcal{L}_2 closed system contribution is a state and hence time-dependent $\beta_2(t)$

$$\beta_c(t) = \beta_2(t) = \frac{\langle \hat{H}(t) \hat{S}(t) \rangle}{\langle \hat{H}(t) \hat{H}(t) \rangle}, \tag{53}$$

defined so that the system is closed and heat is not transferred to or from the system, $\dot{Q}(t) = 0$. This choice also makes the closed system follow a path of increasing entropy. That increase of entropy for a closed system signifies that the closed system is dynamically constrained to reorder itself to maximize its entropy. This is Beretta's steepest-entropy-ascent (SEA) quantum thermodynamics, which he recently stipulates as a 4th law of thermodynamics related to general nonequilibrium modeling [6]. Here $\beta_2(t)$ has a highly nonlinear dependence on the density matrix.

In contrast, the above open or Beretta/Bath term \mathcal{L}_3 does involve heat transfer, that is, both energy and entropy exchange between the system and the bath. A better choice for $\beta_3(t)$ involves the following specific entropy evolution.

4.4. Entropy evolution

Let us now consider the time evolution of the base-e entropy Eq. (29). Eq. (31) gives the time derivative of the entropy as $\frac{d\tilde{S}}{dt} = -\text{Tr}(\dot{\rho}(t) \log_e \rho(t))$. Inserting the time derivative $\dot{\rho}(t)$ from Eq. (33), we again get no change from the unitary term, just from the dissipative \mathcal{L} terms:

$$\begin{aligned} \dot{\tilde{S}}(t) &\equiv \text{Tr}(\dot{\rho}(t)\tilde{S}) = \text{Tr}(\dot{\rho}(t)\hat{S}) \\ &= \text{Tr}(\mathcal{L}\hat{S}). \end{aligned} \tag{54}$$

This is a general result for n_q qubits.

For the Beretta closed \mathcal{L}_2 term, entropy changes according to:

$$\dot{\tilde{S}} = \gamma_2 \text{Tr}(\hat{S}\rho(t)\{\hat{S} - \beta_2(t)\hat{H}(t)\})$$

¹⁶ Beretta et al. use $\langle \hat{H}\hat{H} \rangle \rightarrow \langle \Delta E \Delta E \rangle$, $\langle \hat{H}\hat{S} \rangle \rightarrow \langle \Delta E \Delta S \rangle$ and $\langle \hat{S}\hat{S} \rangle \rightarrow \langle \Delta S \Delta S \rangle$.

$$\begin{aligned} \dot{S} &= \gamma_2 \left\{ \langle \hat{S}\hat{S} \rangle - \beta_2(t) \langle \hat{H}(t)\hat{S} \rangle \right\} \\ \dot{S} &= \gamma_2 \left\{ \langle \hat{S}\hat{S} \rangle - \frac{\langle \hat{H}(t)\hat{S} \rangle^2}{\langle \hat{H}(t)\hat{H}(t) \rangle} \right\}. \end{aligned} \tag{55}$$

Entropy cannot decrease for the Beretta closed term because the Cauchy–Schwarz inequality implies that

$$\langle \hat{S}\hat{S} \rangle \geq \frac{\langle \hat{H}(t)\hat{S} \rangle^2}{\langle \hat{H}(t)\hat{H}(t) \rangle}.$$

For the open \mathcal{L}_3 term

$$\dot{S} = \gamma_3 \left\{ \langle \hat{S}\hat{S} \rangle - \beta_3(t) \langle \hat{H}(t)\hat{S} \rangle \right\}. \tag{56}$$

Setting the entropy-rate to energy-rate ratio to a fixed quantity β_Q , we obtain the condition $\beta_Q = \dot{S}/\dot{Q} = d\tilde{S}/dQ$.¹⁷

$$\frac{\dot{Q}}{\dot{S}} = \frac{\langle \hat{H}(t)\hat{S} \rangle - \beta_3(t) \langle \hat{H}(t)\hat{H}(t) \rangle}{\langle \hat{S}\hat{S} \rangle - \beta_3(t) \langle \hat{H}(t)\hat{S} \rangle} = k_B T_Q = \frac{1}{\beta_Q}, \tag{57}$$

which yields an expression for the state dependence of $\beta_3(t)$:

$$\beta_3(t) = \frac{\langle \hat{S}\hat{S} \rangle - \beta_Q \langle \hat{H}(t)\hat{S} \rangle}{\langle \hat{H}(t)\hat{S} \rangle - \beta_Q \langle \hat{H}(t)\hat{H}(t) \rangle} \tag{58}$$

with fixed value for β_Q . Note the above can be written as

$$\beta_3(t) = \beta_2 \frac{\beta_S - \beta_Q}{\beta_2 - \beta_Q} \tag{59}$$

where we have defined $\beta_S = \frac{\langle \hat{S}\hat{S} \rangle}{\langle \hat{H}(t)\hat{S} \rangle}$. This displays a possible singularity if $\beta_2 \rightarrow \beta_Q$. At such a time the equations require special stiffness handling or avoidance by choice of β_Q .

4.5. Purity evolution

Purity (denoted by the symbol \mathcal{P}), is defined as

$$\mathcal{P}(t) \equiv \text{Tr}(\rho(t)\rho(t)). \tag{60}$$

The rate of change of this purity is given by

$$\dot{\mathcal{P}}(t) = \frac{d\mathcal{P}(t)}{dt} = 2 \text{Tr}(\rho(t)\dot{\rho}(t)). \tag{61}$$

Note that Rényi’s [28–30] generalized form of entropy

$$\mathcal{R}_\alpha[\rho] = \text{Tr} \left[\frac{\rho - \rho^\alpha}{\alpha - 1} \right],$$

yields the Shannon/von Neumann entropy for $\alpha = 1$, while the “Rényi entropy” for $\alpha = 2$ is closely related to the purity $\mathcal{R}_2[\rho] \equiv 1 - \mathcal{P}(t)$.

The purity, as well as the entropy, are functions of the length of the polarization vectors and of the tensor correlations. For example, the purity for one qubit is $\mathcal{P}(t) = \frac{1+P_A^2}{2}$ and $\mathcal{R}_2(t) = \frac{1-P_A^2}{2}$. For two qubits

$$\mathcal{P}(t) = \frac{1 + P_A^2 + P_B^2 + \text{Tr}(T^\dagger T)}{4}$$

¹⁷ k_B is the Boltzmann constant (86.17 $\mu\text{eV}/\text{Kelvin}$), where $\mu\text{eV} = 10^{-6} \text{ eV}$.

$$\mathcal{R}_2(t) = \frac{3 - P_A^2 - P_B^2 - \text{Tr}(T^\dagger T)}{4}. \tag{62}$$

For one qubit on the Bloch ball the von Neumann entropy \mathcal{R}_1 is zero, \mathcal{R}_2 is 0 and the purity is one. For polarization vectors inside the Bloch ball, the entropy is increased and the purity decreased. The purity \mathcal{P} ranges from 1 to $1/2^{nq}$.

Using Eq. (32), we find that the purity is unchanged by the unitary term, but is altered by the Lindblad terms. For both the open and closed $\mathcal{L}_2, \mathcal{L}_3$ cases, the purity displays a steady decrease but especially for the Lindblad noise control term \mathcal{L}_1 an increase is likely (see later). Consider

$$\begin{aligned} \dot{\mathcal{P}}(t) &= 2 \text{Tr}[\rho(t)\mathcal{L}_1] \\ &= 2 \gamma_1 \text{Tr}[\rho(t)L(t)\rho(t)L^\dagger(t) - \rho(t)\rho(t)L^\dagger(t)L(t)] \\ &= \gamma_1 \text{Tr}[\rho(t)\rho(t)[L(t), L^\dagger(t)] - [\rho(t), L(t)]^\dagger[\rho(t), L(t)]]. \end{aligned} \tag{63}$$

The trace property $\text{Tr}(AB) = \text{Tr}(BA)$ was again invoked to generate the above results. The last part puts the purity expression in Lidar form [31]. To assure that purity decreases $\dot{\mathcal{P}}(t) \leq 0$ we get the condition

$$\text{Tr}[\rho(t)\rho(t)[L(t), L^\dagger(t)]] \leq \text{Tr}[[\rho(t), L(t)]^\dagger[\rho(t), L(t)]], \tag{64}$$

where the right hand side is a positive number. This places a constraint on the Lindblad operators to yield decreasing purity, but increasing Rényi entropy $\mathcal{R}_2[\rho] = 1 - \mathcal{P}^2$. Thus the above restriction to Lindblad operators that decrease purity also satisfies the requirement that the \mathcal{R}_2 entropy increases. Since the Shannon entropy \mathcal{R}_1 ¹⁸ generally tracks \mathcal{R}_2 , we can use the above condition on L to give increased entropy. Note that condition (64) is always satisfied when $L(t)$ is Hermitian [31,32].

However, if we use non-Hermitian Lindblad operators that violate the above condition (64), we could decrease entropy, and such Lindblads will tend to undo some chaos and impose order. Later we will invoke this possibility as a method for noise compensation.

4.6. Equilibrium

We assume that the spin-spin and the Rabi terms of the Hamiltonian are turned off at some time and the Hamiltonian at the equilibrium time t_f is of diagonal form $H_f \rightarrow H_0$. In that limit the unitary term vanishes $[\rho_G, H_f] = 0$, since the Gibbs density matrix is a function of H_f and β_g .

$$\begin{aligned} \rho_G &= \frac{e^{-\beta_g H_f}}{Z} \\ Z &= \text{Tr}(e^{-\beta_g H_f}). \end{aligned} \tag{65}$$

In the equilibrium (Gibbs density matrix) limit at final time $t \rightarrow t_f$, $\beta_2(t_f) \rightarrow \beta_g$, for a closed system and $\beta_3(t_f) \rightarrow \beta'_g$, for an open system. The final equilibrium temperature $T_g = k_B/\beta'_g$ for an open system case is arrived at by evolving along a path of steepest-entropy-ascent (SEA). Note that in the equilibrium limit both \dot{S} and \dot{Q} vanish as expected. The temperature T_g , which can be associated with a bath in equilibrium, is not the same as T_Q . It nevertheless leads to an associated equilibrium temperature $1/\beta'_g = T_g$ as determined by the SEA dynamics and the initial state.

Note that negative absolute temperatures and thus negative β_g values can result since we have a bounded spectrum as discussed in [33–35].

The role of the fixed quantity β_Q appears during the process and determines $\Delta S = \beta_Q \Delta Q$, where for finite increments are

$$\Delta S = \int_{t_1}^{t_2} dt \dot{S}(t)$$

¹⁸ These are base e logs. Divide by Log(2) to convert to base 2 logs.

and

$$\Delta Q = \int_{t_1}^{t_2} dt \dot{Q}(t).$$

Here the t_1, t_2 interval encompasses regions where entropy changes occur. Thus β_Q fixes the ratio between the entropy and the energy exchanged during the process between the system and the bath by means of their heat interaction.

4.7. Semi-positive definite property of Lindblad

The positive-definite property of the density matrix implies that each of the density matrix eigenvalues are positive or zero. An initial density matrix is assured to be positive-definite by having inside the Bloch ball observables. Beretta has provided a proof that for $\mathcal{L}_2, \mathcal{L}_3$ the semi-positive character will persist dynamically and here we confirm the validity of that requirement.

5. Model master equation results

The major components of this study are relegated to several appendices. Using those studies as a resource, we present the case of a CNOT gate for an open and then a closed system, first with no noise and then with noise. We also consider the approach to equilibrium as dictated by Lindblad–Beretta (SEA) dynamics. There follows an examination of possible ways to ameliorate the destructive effects of noise with emphasis on noise during the gate.

Extension of this study to the dynamics of the two qubit SWAP gate, to the formation of Bell states, and to the Toffoli gate, inter alia, are provided separately in the form of Mathematica packages [36–38]. The distribution of these codes is done in the hope that they might be useful in testing various noise correction and noise compensation scenarios.

5.0.1. CNOT gate with noise and noise compensation – open system

No environment is an island unto itself.¹⁹ An environment is entangled with a quantum system, which can be a problem if it forces the system to be classical or sends noise, but can be a resource if it sends increased purity. Indeed, error correction methodology involves setting up a system of qubits that get entangled with a quantum system, without destroying it, and then sends a well-informed curative signal back to the quantum system through its entanglement. Here the environment itself plays that role. That idea is realized here by hand-designed Lindblad operators. They are designed for each type of gate to enhance purity and thus decrease entropy and reduce chaos, without being destructive even when there is little or no noise. Developing such environment-based realistic signals is a major challenge that will be explored in subsequent publications.

It should be noted that the requirement for steepest-entropy-ascent (SEA) is applied to cases without noise or noise compensation. Clearly noise generally causes an increase in entropy above SEA, whereas noise compensation can push the ascent to be lower and even to go below SEA.

As shown later, the SEA contribution to say a CNOT gate can be quite destructive. Therefore, gates need to be performed well before the onset of the ultimate SEA, which plays an essential role in the ultimate equilibrium state, but needs to be on but minimized during gate operations. Therefore, we first examine the case of a CNOT gate with noise and noise compensation for zeroed SEA, $\gamma_3 \rightarrow 0$. Limits on a tolerable SEA effect will be examined thereafter.

The Lindblad noise and noise compensation setup is described in [Appendix D](#), along with details about the pulses that turn on the gates. A typical example of the random noise pulses is shown in [Fig. D.21](#).

The main result of this study is shown in [Fig. 10](#). In this plot, we see the noise pulses (distributed over the gate-on interval) and the noise correction taps (close vertical lines), The evolution for the z-polarization of qubit B $P_z^B(t)$ is shown as going from -1 to 1 as expected for a CNOT gate with

¹⁹ With apology to John Donne.

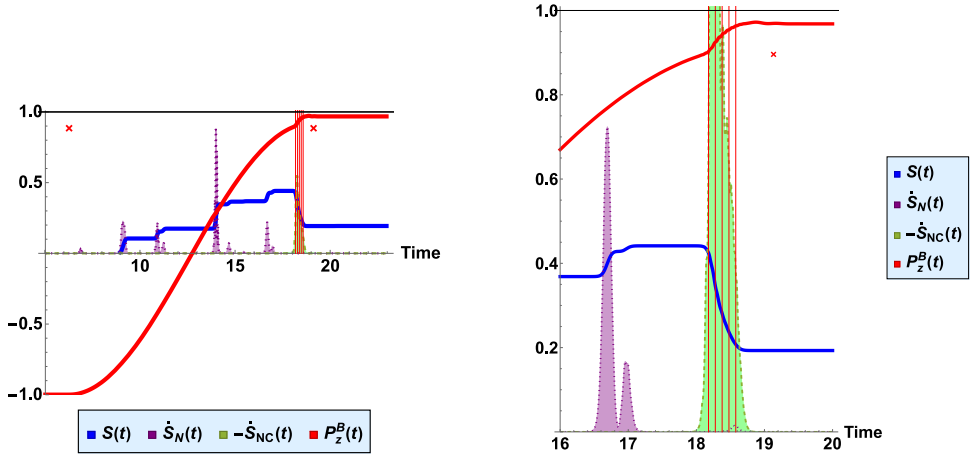


Fig. 10. The effect of noise (N) and noise compensation (NC) on the entropy (S) and z-component polarization of qubit B (P_z^B), for a CNOT gate with control qubit A. Here P_z^B (red) and S (blue) are shown as solid curves. The entropy rate of change for the NC is shown as $-\dot{S}_{NC}$ (green) in the zone of final NC taps, whereas the entropy rate of change for the noise (N) is shown as \dot{S}_N (purple). Since \dot{S}_N is positive, it increases entropy. The negative value of \dot{S}_{NC} decreases entropy and pushes P_z^B closer to where it should be in the noiseless case. The RHS plot is a closer look, where clearly N increases while NC decreases entropy. This demonstrates the basic dynamics of selecting a purity increasing Lindblad operator to partially cancel noise. The results here are obtained by fine tuning parameters with $\Gamma_N = \Gamma_{NC} = 0.2 \approx \omega_2$. For N and NC both off, the CNOT fidelity is 99.99%, with noise only it reduces to 94%, but is lifted back up to 98% by NC. The SEA term is minimized by taking $\gamma_3 \ll \omega_2$. This is a partial reduction of noise based on an estimate of the expected noise as guided by a computed simulation. The red X marks the start and stop of the Rabi pulse.

control on qubit A. The weak noise and noise compensation curves have been scaled up for visibility. The jagged entropy curve shows how random noise pulses increase the entropy during the gate, but the noise compensation pulses bring the entropy down, and the value of $P_z^B(t)$ is pushed back up to where it should be without the noise. This is the essential idea of how to use noise compensation to make up for the noise during the gate. The LHS plot is just a closer look during the correction taps.

Fig. 11 shows the fidelity of the CNOT gate with control on qubit A as a function of the overall noise strength Γ_N . Without noise, it is a horizontal curve at the 99.9% level, then the fidelity dives to the 94% level (bottom curve), but is lifted back up to the 98% level by the noise compensation. There are two versions of the noise compensation settings; the higher curve is for a constant sizable value of the Γ_{NC} overall strength which works best for stronger noise, and the other uses a weaker overall Γ_{NC} strength for the weaker noise region.

It is seen here that there is a partial but significant restoration of entropy provided by the Lindblad noise compensation taps, but not a complete correction. Improved designs, perhaps using chirp taps or better timing can improve these results in any case with these taps, a very simplified less demanding version of noise control protocols could close the gap. That needs to be explored.

5.0.2. SWAP gate and bell state with noise and noise cancellation – open system

The SWAP Gate and Bell State dynamics with Noise and Noise cancellation for an open system parallels the prior discussion as can be explored by accessing the QCPIIT codes. The distribution of noise and noise cancellation pulses is of course is more intricate.

5.0.3. SEA effect on gates

Here we see the SEA effect on a CNOT gate. The dependence of a CNOT gate's fidelity on the value of γ_3 for an open system without noise or noise compensation is shown in Fig. 12 for three values of γ_3 . A value of $\gamma_3 \approx .02$ is barely tolerable in the sense that the CNOT gate had a fidelity of

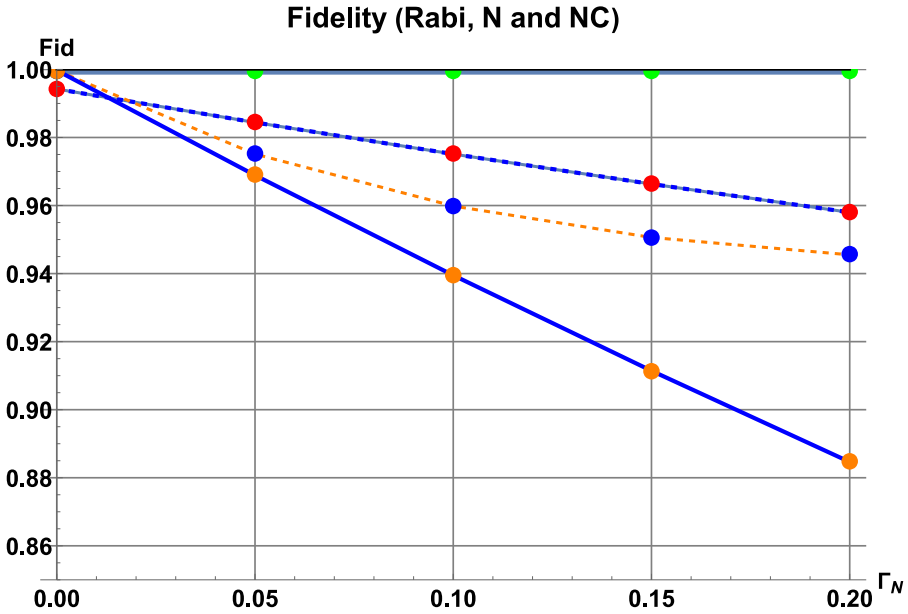


Fig. 11. Fidelity of the CNOT gate versus the overall noise strength Γ_N . The top horizontal curve at the 99.9% level is for no noise. The bottom curve is with noise, yielding CNOT gate fidelity at the 94% level. Noise compensation lifts the CNOT gate fidelity back up to the 98%–96% level as shown in the two middle curves. The upper middle curve uses a constant strong Γ_{NC} and the lower middle uses a weaker Γ_{NC} in the low noise region.

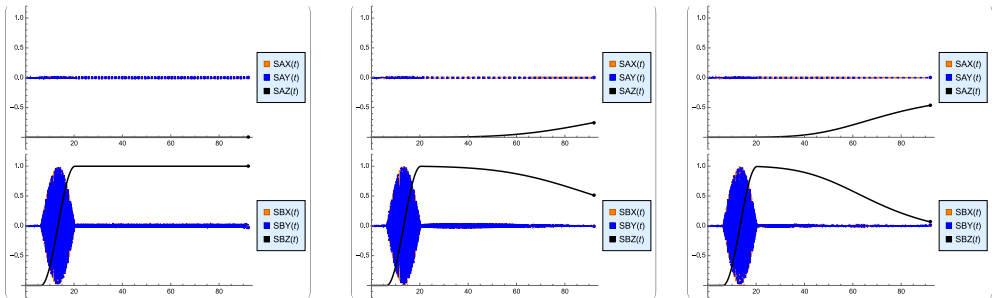


Fig. 12. CNOT gate spin observables for unitary plus SEA open system evolution; e.g., no noise or noise compensation terms. Here initial state case $|11\rangle$ and final state is very close to $|10\rangle$. The CNOT appears during the 10 to 20 ns interval, with a fidelity of 99.96% for $\beta_3 = .003$. Here $\beta_0 = 1/12$ is used. For the LHS there is negligible SEA $\gamma_3 = .003$, whereas for the middle $\gamma_3 = .01$ and RHS $\gamma_3 = .03$ plots the fidelity is reduced as shown in Fig. 13.

99.89%, which places a constraint on the gate versus SEA dynamics. Equilibrium is not established until much later times $\approx 1/\gamma_3$.

The general condition suggested by these results is that $\omega_2 \gamma_3 \ll \frac{0.3}{n_g}$, for n_g gates in order to minimize the effect of SEA on the action of the gates.

The establishment of Gibbs equilibrium occurs at the final time t_g , where $\beta_3(t_g) \equiv \beta_2(t_g)$ and the density matrix assumes the standard Gibbs diagonal form. In that limit the x and y polarizations go to zero and only the z -component polarizations and spin correlation take on their equilibrium values. The Rabi driving term and the spin–spin interaction acted earlier to produce the CNOT gate and then turned off, whereupon the SEA controls the ultimate equilibrium state as determined

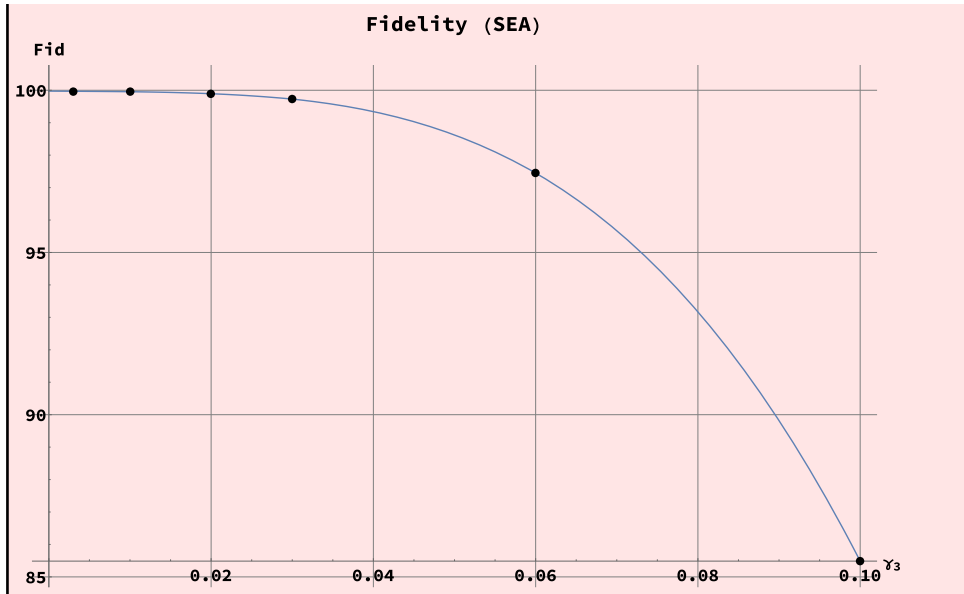


Fig. 13. CNOT gate Fidelity versus SEA strength γ_3 for $\beta_Q = 1/12$. Case is as in prior figure with control for CNOT on qubit A. To keep the SEA effect from being too detrimental, even before the introduction of noise, we must design a system with β_3 below .03.

by the γ_3 and β_Q parameters. The CNOT parameters are the strength of the driving term ω_2 , the resonance frequency ω and the spin–spin interaction strength J , along with the ω_A^L, ω_B^L splitting. The essential point is to design the system so that the CNOT is done with earlier than the times associated with the SEA and equilibrium regions; thus, we require that γ_3 is much smaller than ω_2 . In addition, we prefer to avoid the β_Q close to β_2 region during the dynamic evolution to circumvent the stiffness issue.

6. Conclusions

The Lindblad–Beretta model equations for the evolution of the density matrix have been applied to four-level systems that implement non-spatially-separable two-qubits, including single and double qubit gates and the requirement of steepest entropy ascent for open and closed systems. Noise and noise compensation effects have been examined with a focus on the CNOT gate. The detrimental effects of noise can be alleviated by carefully designed Lindblad taps to partially restore the CNOT gate. The basic noise compensation idea is analogous to magnetizing an iron rod placed parallel to a magnetic field by tapping it. The result is to decrease entropy by increasing order.

More work is required to enhance the noise compensation by designing explicit electromagnetic taps for a variety of gates and to ascertain if such steps can reduce the burden and simplify noise correction protocols.

After completion of our study, an earlier excellent paper suggesting that purity increasing Lindblad operators can help to stabilize an open quantum system was found. That citation [39] encourages us to believe we are on the right track to advocate use of Lindblad taps to compensate for errors.

Several very insightful papers where Beretta’s SEA idea has been examined in a variety of interesting ways are in [40–42]. For papers that deal with related matters, such as studies of noise and of methods for solving the Lindblad equation see [43–47].

Here the focus is on local two-qubit dynamics with noise and noise cancellation. Future developments will complete the study by addressing non-local effects as needed to model two-qubit implementations that involve spatial separation and isolation, by substituting the single-system formulation of steepest-entropy-ascent (SEA) non-equilibrium quantum thermodynamics used here with the composite-system formulation originally developed for such purpose by Beretta in [9,10,13], implemented in [8,48] and recently emphasized in the context of no-signaling in nonlinear extensions of quantum dynamics in [27].

CRedit authorship contribution statement

Frank Tabakin: Conceptualization, Methodology, Software, Writing – original draft, Visualization, Investigation, Supervision, Writing – review & editing.

Declaration of competing interest

The authors declare that they have no known competing financial interests or personal relationships that could have appeared to influence the work reported in this paper.

Data availability

No data was used for the research described in the article.

Acknowledgments

The author wishes to thank Rohit Kishan Ray and the referee for their important insights and highly constructive suggestions.

Appendix A. One-qubit Rabi resonance

Insight into how a Rabi resonance [49] can produce a quantum gate is presented here. The single qubit density matrix is specified by the time dependence of the polarization vector $\vec{P}(t)$. An exact solution for the one-qubit density matrix and associated polarization vector is obtained by applying two rotations about two axes as described in the original Rabi oscillation paper [49].

A rotating wave approximation (RWA) simulates the exact treatment of unitary evolution with a time-dependent Hamiltonian, that is fully accomplished using a time-ordered unitary operator. A simple truncation of the full time-ordered product does not suffice to represent a unitary operator, which motivates using the RWA, as described clearly in [50]. Using a simplified version of the driving term is also part of the RWA because the driving signal is usually only approximately of the simple rotating magnetic field form used here.

In preparation for later use, consider how a rotation, specified by a time-dependent unitary operator $U(t)$, transforms an initial density matrix $\rho_1(t)$ to a new density matrix $\rho_2(t) = U(t)\rho_1(t)U^\dagger(t)$. Taking a time derivative and setting \hbar to one, we obtain²⁰

$$\begin{aligned}
 & \dot{\rho}_2(t) && \text{(A.1)} \\
 & = \dot{U}\rho_1(t)U^\dagger(t) + U(t)\rho_1(t)\dot{U}^\dagger(t) + U(t)\dot{\rho}_1(t)U^\dagger(t) \\
 & = \dot{U}(t)U^\dagger(t)\rho_2 + \rho_2U(t)\dot{U}^\dagger(t) + U(t)\dot{\rho}_1(t)U^\dagger(t) \\
 & = [\dot{U}(t)U^\dagger(t), \rho_2] - i[U(t)H_1(t)U^\dagger(t), \rho_2] \\
 & \quad \dot{\rho}_2(t) = -i[H_2(t), \rho_2(t)] \\
 & \quad H_2(t) \equiv U(t)H_1(t)U^\dagger(t) + i\dot{U}(t)U^\dagger(t) .
 \end{aligned}$$

²⁰ The dot denotes a time derivative and $[A, B]$ is a commutator.

We have invoked $\frac{d}{dt}(U^\dagger(t)U(t)) = 0$. The new density matrix ρ_2 and Hamiltonian H_2 are defined in the rotated frame.²¹

A simpler derivation uses the Schrödinger equation:

$$\begin{aligned}
 H_1(t)|\psi_1(t)\rangle &= i|\dot{\psi}_1(t)\rangle & (A.2) \\
 \left[U(t)H_1(t)U^\dagger(t)\right]U(t)|\psi_1(t)\rangle &= iU(t)|\dot{\psi}_1(t)\rangle \\
 = i\frac{d}{dt}(U(t)|\psi_1(t)\rangle) - i\dot{U}(t)U^\dagger(t)U(t)|\psi_1(t)\rangle \\
 H_2(t)|\psi_2(t)\rangle &= i|\dot{\psi}_2(t)\rangle,
 \end{aligned}$$

with $|\psi_2(t)\rangle = U(t)|\psi_1(t)\rangle$.

This shows how to generate the density matrix and Hamiltonian in a rotating frame defined by a unitary operator $U(t)$. Note that although the transformation is generated by a unitary operator, due to the time dependence of U , it is not a canonical transformation, the energy spectrum is not preserved. We get a new Hamiltonian. Transformation to a rotating frame is a change in view. We will apply these general steps to one and two-qubit systems next. These properties also apply to a second rotation and also to multi-qubit systems.

A.1. NOT gate case

Consider a one-qubit Hamiltonian²² with non-degenerate levels plus a Rabi driving term:

$$\begin{aligned}
 H(t) &\equiv -\frac{\hbar\omega_L}{2}\sigma_z + \frac{\hbar\omega_2}{2}(\cos(\omega t)\sigma_x - \sin(\omega t)\sigma_y) & (A.3) \\
 &= \frac{\vec{\Omega}_0(t) \cdot \vec{\sigma}}{2}
 \end{aligned}$$

$$\vec{\Omega}_0(t) = \omega_2(\cos(\omega t)\hat{x} - \sin(\omega t)\hat{y}) - \omega_L\hat{z} \tag{A.4}$$

This Hamiltonian produces a pure NOT gate in a rotating frame as shown later. The Rabi driving term of strength ω_2 arises from rotating a magnetic field in the x–y plane with an angular frequency of ω . The time evolution of the polarization vector in the original (lab) frame is obtained from

$$\begin{aligned}
 \frac{d\vec{P}(t)}{dt} &= \text{Tr}(\vec{\sigma} \dot{\rho}(t)) = -\frac{i}{\hbar}\text{Tr}(\vec{\sigma} [H(t), \rho(t)]) & (A.5) \\
 &\equiv \vec{\Omega}_0(t) \times \vec{P}(t) \\
 \dot{P}_x(t) &= \omega_L P_y(t) - \omega_2 P_z(t) \sin(\omega t) \\
 \dot{P}_y(t) &= -\omega_L P_x(t) - \omega_2 P_z(t) \cos(\omega t) \\
 \dot{P}_z(t) &= +\omega_2 (P_y(t) \cos(\omega t) + P_x(t) \sin(\omega t)).
 \end{aligned}$$

The magnitude of the polarization vector P is a constant:

$$\frac{dP(t)}{dt} = \frac{1}{2}\vec{P}(t) \cdot \frac{d\vec{P}(t)}{dt} = \frac{1}{2}\vec{P}(t) \cdot (\vec{\Omega}_0(t) \times \vec{P}(t)) = 0.$$

The above coupled equations describe a spin precessing about a moving $\vec{\Omega}_0(t)$ axis.

A.1.1. First rotation

Following the original Rabi resonance paper [49], a sequence of rotating frames are invoked to solve these equations. A unitary operator $U_1(t) \equiv e^{-\frac{i}{2}\omega\sigma_z t}$, transforms to a frame rotating about

²¹ For $U(t) \rightarrow e^{i\mathbf{v}t}$, $H_2(t) \rightarrow U(t)H_1(t)U^\dagger(t) - \mathbf{v}$, with \mathbf{v} a Hermitian operator.

²² We now denote the laboratory frame Hamiltonian $H_1(t)$ simply as $H(t)$.

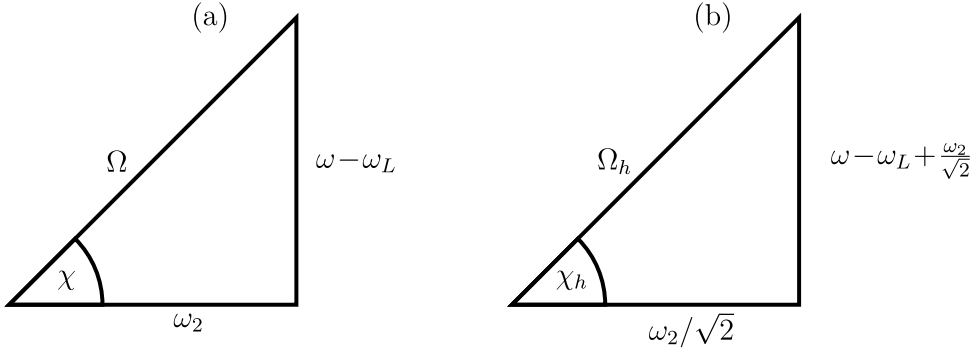


Fig. A.14. The components of $\vec{\Omega}$ for the (a) NOT and the (b) Hadamard one-shot gates. Note that at resonance $\omega \equiv \omega_L$, the angle $\chi \equiv 0$ and the angle $\chi_h \equiv \frac{\pi}{4}$.

the z-axis with an angular frequency ω . The Hamiltonian in the rotating frame H_2 is obtained from the above general rule as: $H_2 \equiv U_1(t)H(t)U_1^\dagger(t) + i \dot{U}_1(t)U_1^\dagger(t)$:

$$H_2 = \frac{\omega - \omega_L}{2} \sigma_z + \frac{\omega_2}{2} \sigma_x = \frac{\vec{\Omega} \cdot \vec{\sigma}}{2}, \tag{A.6}$$

with $\vec{\Omega} \equiv (\omega - \omega_L)\hat{z} + \omega_2\hat{x}$. Note that in this rotating frame the Hamiltonian H_2 is time-independent with a pure NOT gate.

The magnitude of $\vec{\Omega}$ is $\Omega \equiv \sqrt{(\omega - \omega_L)^2 + \omega_2^2}$. The following coupled equations:

$$\begin{aligned} \frac{d\vec{P}(t)}{dt} &= \vec{\Omega} \times \vec{P}(t) \\ \frac{dP_x(t)}{dt} &= -(\omega - \omega_L)P_y(t) \\ \frac{dP_y(t)}{dt} &= +(\omega - \omega_L)P_x(t) - \omega_2 P_z(t) \\ \frac{dP_z(t)}{dt} &= +\omega_2 P_y(t) \end{aligned} \tag{A.7}$$

describe the polarization \vec{P} in the first rotating frame. The length of the polarization vector in the rotating frame is still constant and it precesses about the fixed vector $\vec{\Omega}$ which defines a new axis of precession in the x-z plane.

A.1.2. Second rotation

A second rotation using that new axis of precession is generated by $U_2(t) = e^{+i\frac{1}{2}\vec{\Omega} \cdot \vec{\sigma} t}$, which yields a new Hamiltonian $H_3 = 0$, and thus to a fixed polarization vector \vec{p} in the second rotation frame. The direction of the second rotation is defined by $\Omega \sin(\chi) = (\omega - \omega_L)$ and $\Omega \cos(\chi) = \omega_2$, and its magnitude as $\Omega \equiv \sqrt{(\omega - \omega_L)^2 + \omega_2^2}$ as shown in Fig. A.14.

A.1.3. Solution

The fixed density matrix in the second rotating frame is then time independent: $\rho_3 = \frac{1}{2}(\sigma_0 + \vec{p} \cdot \vec{\sigma})$, where \vec{p} is the fixed initial polarization. From ρ_3 , we rotate back to the first rotation frame density matrix $\rho_2 = U_2^\dagger(t)\rho_3 U_2(t)$ to determine a solution for the polarization vectors in the first rotation

frame $\vec{P}(t)$:

$$\begin{pmatrix} P_x(t) \\ P_y(t) \\ P_z(t) \end{pmatrix} = M(t) \cdot \begin{pmatrix} p_x \\ p_y \\ p_z \end{pmatrix}, \tag{A.8}$$

where $M(t)$ is the matrix

$$\begin{pmatrix} \cos^2(\chi) + \sin^2(\chi) \cos(\Omega t) & -\sin(\chi) \sin(\Omega t) & \sin(2\chi) \sin(\Omega/2 t)^2 \\ \sin(\chi) \sin(\Omega t) & \cos(\Omega t) & -\cos(\chi) \sin(\Omega t) \\ \sin(2\chi) \sin(\Omega/2 t)^2 & \cos(\chi) \sin(\Omega t) & \sin^2(\chi) + \cos^2(\chi) \cos(\Omega t) \end{pmatrix}.$$

The vector $(P_x(t), P_y(t), P_z(t))$ equals $\vec{p} = p_x, p_y, p_z$ at time $t = 0$. At the Rabi resonance value of $\omega \rightarrow \omega_L$ we get $\Omega \rightarrow \omega_2$ and $\chi \rightarrow 0$. For this on-resonance case, we get a simple rotation about the \hat{x} axis.

$$\begin{pmatrix} P_x(t) \\ P_y(t) \\ P_z(t) \end{pmatrix} = \begin{pmatrix} 1 & 0 & 0 \\ 0 & \cos(\omega_2 t) & -\sin(\omega_2 t) \\ 0 & \sin(\omega_2 t) & \cos(\omega_2 t) \end{pmatrix} \cdot \begin{pmatrix} p_x \\ p_y \\ p_z \end{pmatrix} \tag{A.9}$$

Now we invoke a Rabi pulse time $t_p = \pi/\omega_2$ called a π pulse. At that Rabi pulse time t_p the polarization vector in the first rotating frame is exactly that of a NOT gate:

$$\{p_x, p_y, p_z\} \xrightarrow{\text{NOT}} \{p_x, -p_y, -p_z\}.$$

Rotating back to the original frame involves one more reverse transformation $\rho = U_1^\dagger(t) \rho_2 U_1(t)$ which yields the laboratory frame solution.

For an initial state $\{p_x, p_y, p_z\} = \{0, 0, p_z\}$ from Eq. (A.8) the final z polarization is

$$P_z(t) = p_z \left(1 - 2 \frac{\omega_2^2}{\Omega^2} \sin^2\left(\frac{\Omega t}{2}\right) \right),$$

which is the standard result. At resonance and at time $t_p = \pi/\omega_2$, the result is a simple flip or NOT gate $P_z(t_p) = -p_z$.

The evolution of the polarization at the Rabi resonance in the first rotation and original lab frames for the case of a pure one-qubit NOT gate are shown in Fig. A.15.

Far from resonance, $\chi \rightarrow \pi/2$, and $M(t)$ reduces to a rapid rotation about the z-axis. The z-polarization then is fixed, and for small initial polarizations in the x-y plane, the result is a narrow precession cone. This essentially turns off the Rabi resonance. It is this basic mechanism that provides the selectivity for the controlled gates later.

A.1.4. Pulses

Parts of the Hamiltonian $H(t)$ are turned on and off using electromagnetic pulses to produce gates. Error functions (erf) are used to produce steady, sharp and continuous switches²³:

$$\theta_{\text{on}}(t, t_a) = \frac{1}{2} \{1 + \text{erf}[(t - t_a)/\tau_a]\}, \quad \theta_{\text{off}}(t, t_b) = \frac{1}{2} \{1 + \text{erf}[(t_b - t)/\tau_b]\},$$

where t_a, t_b are the turn on and off times with associated widths τ_a, τ_b ²⁴ An on/off switch over an interval is:

$$\theta(t, t_a, t_b) = \theta_{\text{on}}(t, t_a) \theta_{\text{off}}(t, t_b).$$

For example, a controlled gate involves turning on the nondegeneracy or Larmor frequency part of the Hamiltonian, then the splitting term and finally the Rabi term, with reversed order for the turn-offs. For example, for the one qubit case which does not have a spin-spin term, we use $\omega_L(t) = \omega_L \theta(t, t_a, t_b)$ to turn on the Larmor frequency and both $\omega_2(t) = \omega_2 \theta(t, t_c, t_d)$ and $\omega(t) = \omega \theta(t, t_c, t_d)$ to turn on the Rabi. This pulse sequence is illustrated in Figs. A.16 and A.17

²³ At times we use an tanh based pulse.

²⁴ We typically set $\tau = \frac{t_b - t_a}{n}$, with $n \geq 150$ to produce rapid but smooth pulses.

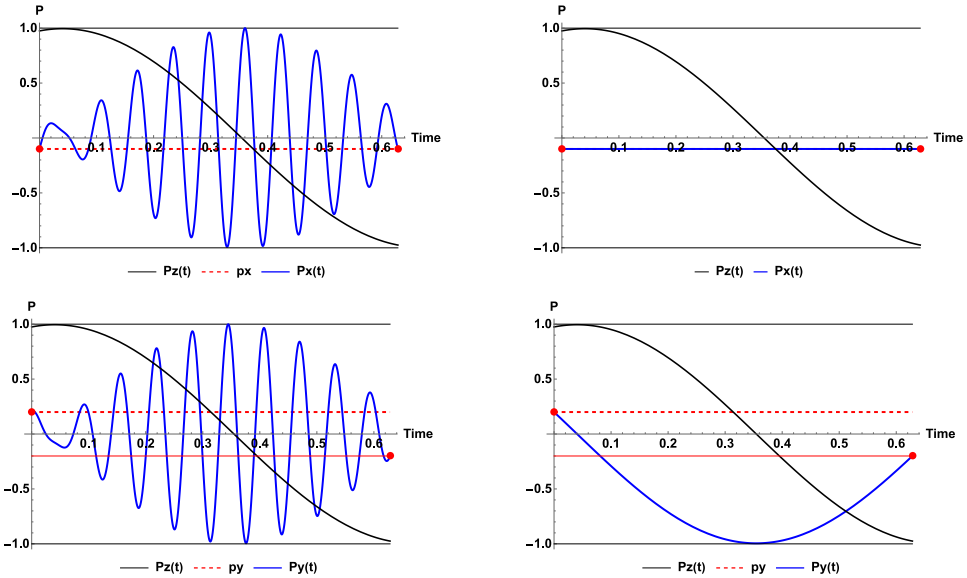


Fig. A.15. Polarization evolution for a single non-degenerate qubit at the Rabi resonance ($\omega \equiv \omega_L$) with a π pulse of duration $t_p = \pi/\omega_2$. Not gate case: in the laboratory (left) and first rotating (right) frames. The angular frequency is taken to be $\omega_L = 100$ GHz and the strength of the Rabi driving term is $\omega_2 = \omega_L/40$. The horizontal dashed line indicates the flipped $-p_y$ value. In the laboratory frame the x and y polarizations oscillate with the period $T_L = 0.0628$, which is smaller than the driving period $T_2 = 1.25664$. The envelope of the x, y polarizations arises from the fixed length of the total polarization. Units of time are defined by $\hbar = 1$.

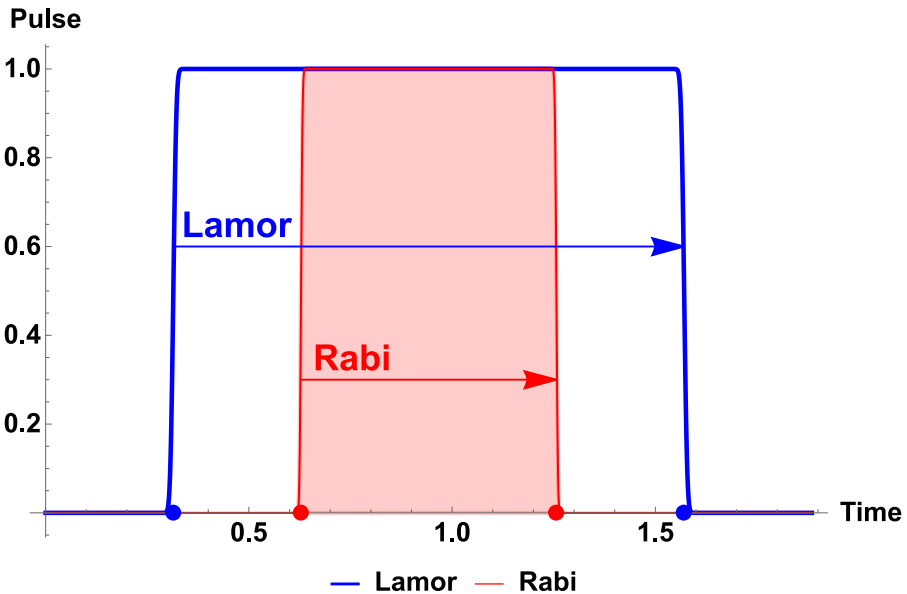


Fig. A.16. Pulses for Larmor in blue: $\{t_a, t_b, \tau_H\} = \{0.31415, 1.57080, 0.00838\}$ and for Rabi in red: $\{t_c, t_d, \tau_R\} = \{0.62832, 1.25664, 0.00419\}$.

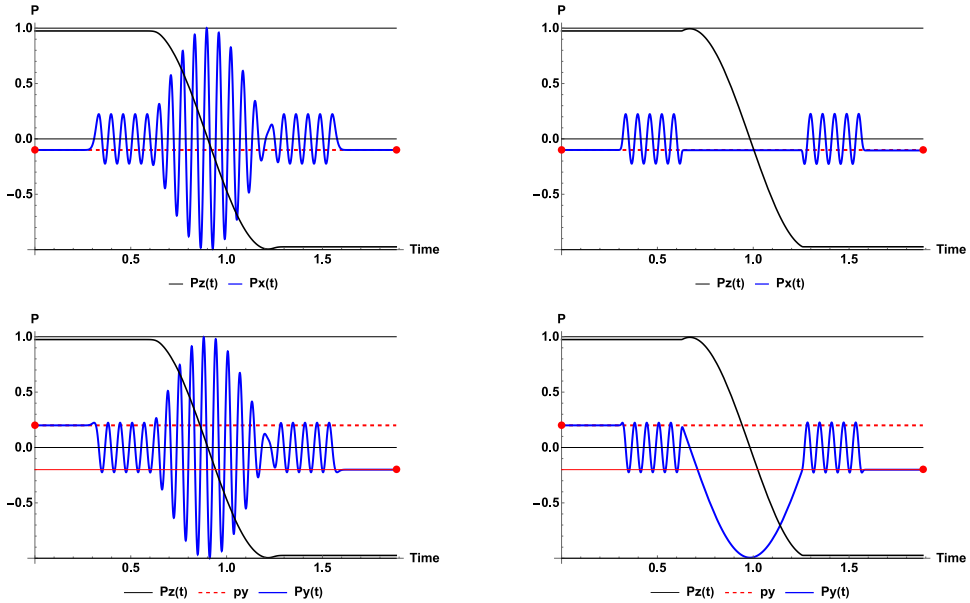


Fig. A.17. Pulsed version of Fig. A.15, where during the initial time of $5 T_L$ there is degeneracy and no precession, then the Larmor precession is turned on for a period of $5 T_L$ and then the Rabi driving term is applied for the π pulse time. This is followed by a turn-off of the Larmor precession and finally of the level splitting. These steps will be applied in the two-qubit case later.

A.2. Hadamard gate case

The prior steps can be modified to generate a Hadamard by use of a Rabi resonance. A $\pi/2$ pulse in the first rotation frame is not the same as a pure Hadamard gate for which $\{p_x, p_y, p_z\} \xrightarrow{\text{Hadamard}} \{p_z, -p_y, p_x\}$. It can be adjusted to replicate a pure Hadamard by additional gates, but it is simpler to develop a one-shot Hadamard setup. Such a setup is obtained by using Hamiltonian

$$H'(t) \equiv -\frac{\hbar \omega_L}{2} \sigma_z + \frac{\hbar \omega_2}{2} \left(\cos(\omega t) \sigma_x - \sin(\omega t) \sigma_y + \sigma_z \right) / \sqrt{2}. \tag{A.10}$$

This Hamiltonian produces a pure Hadamard gate in a rotating frame. In this Hamiltonian the driving magnetic field is rotating about the z-axis with an angular frequency ω with a fixed component in the z-direction. The length of the total B-field as specified by the value ω_2 is the same as used for the NOT gate, but the magnetic field vector now precesses at an angular frequency ω about the z-axis at a $\pi/4$ angle from that z-axis. This choice is made to facilitate a one-shot Hadamard gate.

The unitary transformation $U_1(t) \equiv e^{+\frac{i}{2} \omega \sigma_z t}$, again transforms to a frame rotating about the z-axis with an angular frequency ω . The Hamiltonian in the first rotating frame \hat{H}' is obtained using $\tilde{H}'(t) \equiv U(t)H'(t)U^\dagger(t) + i \dot{U}(t)U^\dagger(t)$,

$$\hat{H}' = \left(\frac{\omega - \omega_L}{2} + \frac{\omega_2}{\sqrt{2}} \right) \sigma_z + \frac{\omega_2}{\sqrt{2}} \sigma_x = \frac{\vec{\Omega}_h \cdot \vec{\sigma}}{2},$$

with $\vec{\Omega}_h \equiv (\omega - \omega_L + \frac{\omega_2}{\sqrt{2}})\hat{z} + \frac{\omega_2}{\sqrt{2}}\hat{x}$. The magnitude of $\vec{\Omega}_h$ is $\Omega_h \equiv \sqrt{(\omega - \omega_L + \frac{\omega_2}{\sqrt{2}})^2 + \frac{1}{2}\omega_2^2}$. For $\omega \rightarrow \omega_L$, $\vec{\Omega}_h \rightarrow \omega_2$.

The first rotated frame polarization vector \vec{P}' satisfies:

$$\begin{aligned} \frac{d\vec{P}(t)}{dt} &= \vec{\Omega}_h \times \vec{P}(t) \\ \frac{dP_x(t)}{dt} &= -(\omega - \omega_L + \frac{\omega_2}{\sqrt{2}})P_y(t) \\ \frac{dP_y(t)}{dt} &= +(\omega - \omega_L + \frac{\omega_2}{\sqrt{2}})P_x(t) - \frac{\omega_2}{\sqrt{2}}P_z(t) \\ \frac{dP_z(t)}{dt} &= +\frac{\omega_2}{\sqrt{2}}P_y(t) \end{aligned} \tag{A.11}$$

for the polarization \vec{P} . The length of the polarization vector in the rotating frame is fixed and the vector Ω_h defines a new axis of precession.

A second rotation using that new axis of precession $\tilde{U}'_2(t) = e^{+i \frac{1}{2} \vec{\Omega}_h \cdot \vec{\sigma} t}$ yields a new Hamiltonian $\tilde{H}'_3 = 0$, and thus to a fixed polarization vector \vec{p} in the second rotation frame. The direction of the second rotation is defined by $\sin(\chi_h) = (\omega - \omega_L + \omega_2/\sqrt{2})/\Omega_h$ and $\cos(\chi_h) = \frac{\omega_2}{\sqrt{2}}/\Omega_h$. The associated fixed density matrix in the second rotating frame is then $\tilde{\rho}_3 = \frac{1}{2}(\sigma_0 + \vec{p} \cdot \vec{\sigma})$. From $\tilde{\rho}_3$, we rotate back to the first rotation frame density matrix $\hat{\rho}_2(t) = \tilde{U}'^\dagger(t) \tilde{\rho}_3 \tilde{U}'(t)$ to determine a solution for the polarization vectors in the first rotation frame $\vec{P}'(t)$:

$$\begin{pmatrix} P'_x(t) \\ P'_y(t) \\ P'_z(t) \end{pmatrix} = M_h \cdot \begin{pmatrix} p_x \\ p_y \\ p_z \end{pmatrix}, \tag{A.12}$$

where M_h is the matrix

$$\begin{pmatrix} \cos^2(\chi_h) + \sin^2(\chi_h) \cos(\Omega_h t) & -\sin(\chi_h) \sin(\Omega_h t) & \sin(\chi_h) \cos(\chi_h) (1 - \cos(\Omega_h t)) \\ \sin(\chi_h) \sin(\Omega_h t) & \cos(\Omega_h t) & -\cos(\chi_h) \sin(\Omega_h t) \\ \sin(\chi_h) \cos(\chi_h) (1 - \cos(\Omega_h t)) & \cos(\chi_h) \sin(\Omega_h t) & \sin^2(\chi_h) + \cos^2(\chi_h) \cos(\Omega_h t) \end{pmatrix}$$

The vector $(P'_x(t), P'_y(t), P'_z(t))$ equals $\vec{p} = \{p_x, p_y, p_z\}$ at time $t = 0$. The above result is identical to Eq. (A.8), except for the appearance of new Ω_h and χ_h quantities which reflect the new orientation of the driving B-field.

Now at the Rabi resonance value of $\omega \rightarrow \omega_L$, $\Omega_h \rightarrow \omega_2$ and $\chi_h \rightarrow \frac{\pi}{4}$. For this on-resonance case

$$\begin{aligned} P_x(t) &= \frac{P_x}{2} (1 + \cos(\omega_2 t)) - \frac{P_y}{\sqrt{2}} \sin(\omega_2 t) + \frac{P_z}{2} (1 - \cos(\omega_2 t)) \\ P_y(t) &= \frac{P_x}{\sqrt{2}} \sin(\omega_2 t) + p_y \cos(\omega_2 t) - \frac{P_z}{\sqrt{2}} \sin(\omega_2 t) \\ P_z(t) &= \frac{P_x}{2} (1 - \cos(\omega_2 t)) + \frac{P_y}{\sqrt{2}} \sin(\omega_2 t) + \frac{P_z}{2} (1 + \cos(\omega_2 t)). \end{aligned}$$

Now we invoke a π pulse time $t'_p = \frac{\pi}{\omega_2}$. Thus at that Rabi pulse time t'_p the polarization vector in the first rotating frame is exactly that of a Hadamard gate:

$$\{p_x, p_y, p_z\} \xrightarrow{HAD} \{p_z, -p_y, p_x\}.$$

Rotating back to the laboratory frame readily yields the results in the original frame.

The evolution of the polarization at the Rabi resonance in both the first rotation and the original lab frames for the case of a pure one-qubit Hadamard gate are shown in Fig. A.19 (see Fig. A.18).

A.3. Other gates

Other quantum gates can be generated by Rabi resonance techniques. For example, the phase shift gate $R_\phi = \begin{pmatrix} 1 & 0 \\ 0 & e^{i\phi} \end{pmatrix} = P_0 + e^{i\phi} P_1$, where $P_0 = (\sigma_0 + \sigma_z)/2$, $P_1 = (\sigma_0 - \sigma_z)/2$ are spin projection

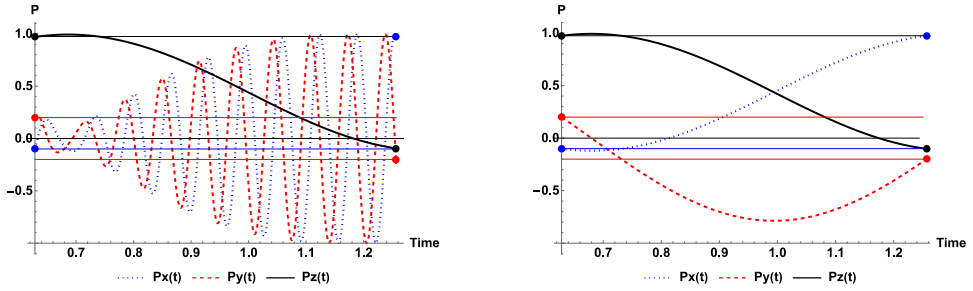


Fig. A.18. Hadamard case: Polarization evolution for a single non-degenerate qubit at the Rabi resonance ($\omega \equiv \omega_L$) with a π pulse of duration $t_p = \pi/\omega_2$. One-shot Hadamard gate case: in the laboratory (left) and (b) in first rotating (right) frame. The angular frequency is taken to be $\omega_L = 100$ GHz and the strength of the Rabi driving term is $\omega_2 = \omega_L/40$. The dashed line indicates the flipped $-p_y$ value. In the laboratory frame the x and y polarizations oscillate with the period $T_L = 0.0628$, which is smaller than the driving period $T_2 = 1.25664$. The envelope of the x , y polarizations arises from the fixed length of the total polarization.

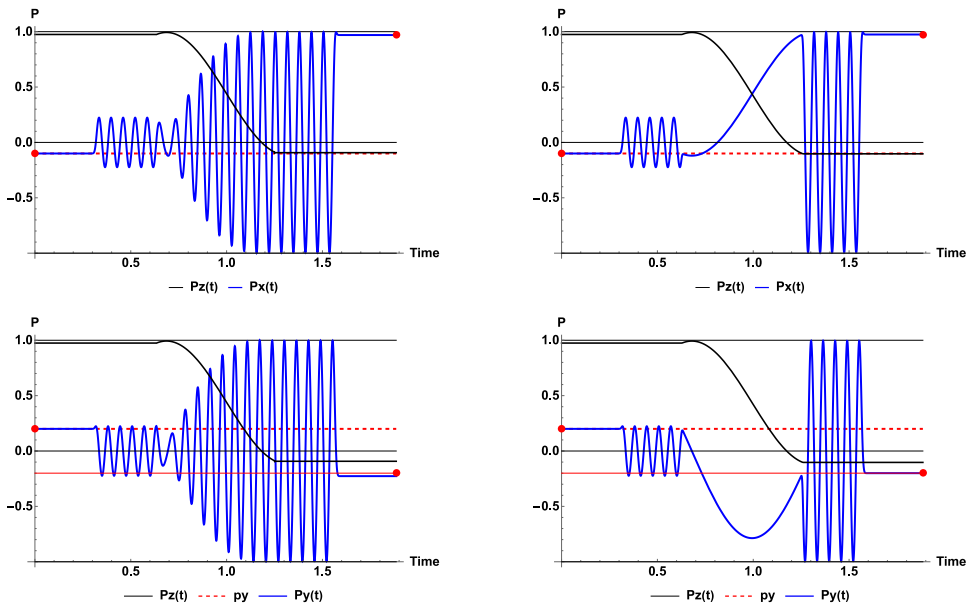


Fig. A.19. Pulsed version for Hadamard see Fig. A.19, where during the initial time of $5 T_L$ there is degeneracy and no precession, then the Larmor precession is turned on for a period of $5 T_L$ and then the Rabi driving term is applied for the π pulse time. This is followed by a turn off of the Larmor precession and finally the level splitting. These steps will be applied in the two-qubit case later.

operators, can be generated by a simple first rotated frame Hamiltonian $H_1 = \frac{1}{2}(\omega - \omega_L + \omega_2)\sigma_z$. At resonance, this is simply a rotation about the z-axis by an angle $\omega_2 t = \phi$, which creates the change $\{p_x, p_y, p_z\} \xrightarrow{\text{Phase}} \{p_x \cos(\phi) - p_y \sin(\phi), p_x \sin(\phi) + p_y \cos(\phi), p_z\}$. That is exactly how R_ϕ affects the one qubit density matrix. A controlled phase operator can then be setup using the procedures discussed herein for the CNOT gate. For $\phi = \pi$ this is a controlled-Z gate. A simple change to the discussion here leads to a controlled-Y gate. Thus a full set of one and two qubit operators can be produced by Rabi resonance methods as is well known. This obviates the need for a bias pulse used in [1].

Appendix B. Two-qubit Rabi resonance

The above discussion can be directly applied to two-qubits in the absence of a spin-spin interaction. The Hamiltonian is then a tensor product sum $H_{AB}(t) = H_A(t) \otimes \mathbf{I}_2 + \mathbf{I}_2 \otimes H_B(t)$, where H_A and H_B can be taken as either the above NOT or Hadamard gate forms or simply cases with zero Rabi driving $\omega_2^A \rightarrow 0$ and/or $\omega_2^B \rightarrow 0$. Here ω_2^A, ω_2^B are the possibly different Rabi driving strengths for qubits A and B. There can also be different frequencies ω_L^A, ω_L^B and thus the prior discussion applies for each qubit separately. Here we take $\omega^A = \omega^B = \omega$, and $\omega_2^A = \omega_2^B = \omega_2$. This reflects the application of the Rabi field over the whole sample.

With two qubits that interact with, for example, a spin-spin interaction, the Rabi oscillations are much more complicated. Driving one qubit affects the other. The extra degeneracy provided by a spin-spin interaction is needed [25] to produce a controlled gate system, so this case is considered next.

Can an analytic or perhaps a good approximate solution to Rabi oscillation for two spin-spin coupled qubits be obtained? In that spirit, the prior steps of two rotations including a spin-spin interaction

$$V_{SS} = \frac{1}{4} (\vec{\sigma}_A \cdot \vec{\sigma}_B - I_4)$$

$$\vec{\sigma}^A \cdot \vec{\sigma}^B \equiv \sum_{i=1,3} \vec{\sigma}_i^A \otimes \vec{\sigma}_i^B. \tag{B.1}$$

are now considered.

B.0.1. First rotation

Applying the first rotation procedure to qubits A and B with the same driving frequency $U_1(t) \equiv e^{+\frac{i}{2}\omega\sigma_z^A t} \otimes e^{+\frac{i}{2}\omega\sigma_z^B t}$, the spin-spin is unchanged. This is a transformation to a frame with static B-fields and pure NOT or pure Hadamard operators. Now let us focus on CNOT gate dynamics. The two-qubit Hamiltonian in the first rotation frame is:

$$H_2 = H_2^A \otimes \sigma_0 + \sigma_0 \otimes H_2^B + V_{SS} \tag{B.2}$$

$$H_2^A = \vec{\Omega}_A \cdot \vec{\sigma} / 2 \quad \& \quad H_2^B = \vec{\Omega}_B \cdot \vec{\sigma} / 2$$

$$\vec{\Omega}^A \equiv (\omega - \omega_L^A)\hat{z} + \omega_2^A \hat{x}$$

$$\vec{\Omega}^B \equiv (\omega - \omega_L^B)\hat{z} + \omega_2^B \hat{x}$$

Here each qubit precesses about its respective $\vec{\Omega}^A$ and $\vec{\Omega}^B$ axis, along with the unchanged spin-spin interaction. This Hamiltonian is time-independent and thus Laplace transformation methods can be invoked. However that involves a 15×15 secular equation inversion which is rather complicated. A Picard iteration method can also be invoked.

In this rotation frame, the time evolution of the 15 spin observables are described by

$$\frac{d}{dt} \vec{P}^A(t) = \vec{\Omega}^A \times \vec{P}^A(t) - \frac{J}{2} \vec{A} \tag{B.3}$$

$$\frac{d}{dt} \vec{P}^B(t) = \vec{\Omega}^B \times \vec{P}^B(t) + \frac{J}{2} \vec{A}$$

$$\frac{d}{dt} \overleftrightarrow{T}(t) = \vec{\Omega}^A \times \overleftrightarrow{T}(t) - \overleftrightarrow{T}(t) \times \vec{\Omega}^B + \frac{J}{2} \vec{\xi} \cdot (\vec{P}^A(t) - \vec{P}^B(t)),$$

where $\vec{\xi} = (\epsilon_{i,j,1}, \epsilon_{i,j,2}, \epsilon_{i,j,3})$, using the Levi-Civita symbol ϵ . Equations for the spin correlation functions \overleftrightarrow{T} can also be obtained involving the nine spin observables:

(1) axial vector

$$\vec{A}(t) = \langle \vec{\sigma}_A \times \vec{\sigma}_B \rangle; \quad A_i(t) = \sum_{j,k=1,3} \epsilon_{ijk} T_{j,k}(t),$$

(2) scalar:

$$S(t) = \langle \vec{\sigma}_A \cdot \vec{\sigma}_B \rangle = \sum_{i,1,3} T_{i,i}(t),$$

and

(3) traceless symmetric form

$$\tau(t) \rightarrow \frac{1}{2}(T_{i,j}(t) + T_{j,i}(t)) - \frac{1}{3}\delta_{ij}S(t).$$

Such equations can provide insights into the dynamical changes.

The (B.3) equations also lead to the results

$$\begin{aligned} \frac{d}{dt}(P_A^2(t) + P_B^2(t)) &= -J(\vec{P}^A(t) - \vec{P}^B(t))\vec{A} \\ \frac{d}{dt}\text{Tr}(\overleftrightarrow{T}^t \overleftrightarrow{T}) &= +J(\vec{P}^A(t) - \vec{P}^B(t))\vec{A}. \end{aligned} \tag{B.4}$$

From $\text{Tr}(\rho^2(t)) = \frac{1}{4}P_A^2(t) + P_B^2(t) + \text{Tr}(\overleftrightarrow{T}^t \overleftrightarrow{T}) \leq 1$, we conclude that $P_A^2(t) \equiv \vec{P}^A(t) \cdot \vec{P}^A(t) \leq 1$, $P_B^2(t) \equiv \vec{P}^B(t) \cdot \vec{P}^B(t) \leq 1$, and $\text{Tr}(\overleftrightarrow{T}^t \overleftrightarrow{T}) \leq 2$. For numerical solutions, we solve the density matrix evolution equations and then display the spin observables.

B.0.2. Second rotation

In this case, invoking a second rotation $U_2(t) = e^{iH_2^A t} \otimes e^{iH_2^B t}$ yields a nonzero Hamiltonian for a nonzero spin-spin interaction ($J \neq 0$):

$$\begin{aligned} H_3(t) &= \frac{J}{4} [\vec{S}^A(t) \cdot \vec{S}^B(t) - \mathbf{I}_4] \\ \vec{S}^A(t) &= e^{iH_2^A t} \cdot \vec{\sigma}^A \cdot e^{-iH_2^A t} \\ \vec{S}^B(t) &= e^{iH_2^B t} \cdot \vec{\sigma}^B \cdot e^{-iH_2^B t}, \end{aligned} \tag{B.5}$$

from which approximate solutions might be based on the exact solution with just V_{SS} . Unfortunately, such steps led to rather complicated expressions and thus direct numerical solutions proved to be more propitious. A useful analytic solution, perhaps based on the precession of each qubit $\vec{S}_\alpha(t) = \vec{\Omega}_\alpha \times \vec{S}(t)$ for $\alpha = A, B$ with the control qubit's axis $\vec{\Omega}^A$ close to the z-axis and the NOT qubit's axis $\vec{\Omega}^B$ close to the x-axis might be possible. Once the spin-spin interaction's effect is included, one could transform back to the second rotation frame and reveal the detailed dynamics. Such information will be gleaned from the numerical results in the main text.

So now return to the main text for the two-qubit CNOT gate results, where the influence of noise, external Bath, and entropy constraints on CNOT dynamics are examined.

B.0.3. Bell state and swap gate cases

To generate the four Bell states, we need to act on qubit A with a Hadamard and then a CNOT gate, with control on qubit A and not on qubit B. We keep the Larmor splitting on. To carry out that sequence we use two different pulse setups. For the Hadamard, we keep the spin-spin off, and set the Rabi frequency $\omega = \omega_A^I$, and use the Hadamard rotating magnetic field, as discussed

in Appendix A.2. Once that is finished, the spin–spin strength is turned on and the Rabi frequency is selected to be $\omega = \delta_{1,1}^{11}$ which generates the CNOT gate. This will be used to track entanglement evolution with noise.

A swap gate is generated by three sequential CNOT gates; namely, $\text{CNOT}(1, 2) \cdot \text{CNOT}(1, 2) \cdot \text{CNOT}(1, 2)$. Thus, with both the full degeneracy and the spin–spin terms on, we use a pulse with $\omega = \delta_{1,0}^{11}$ for a time $\tau = \frac{\pi}{\omega_2}$ followed by $\omega = \delta_{0,1}^{11}$ for the same duration time τ and finally by $\omega = \delta_{1,0}^{11}$ for time τ . A sample result is shown in Fig. 8. This will be used to track swap gate sensitivity to noise.

Appendix C. Toffoli gate and Rabi resonance

The three-qubit Toffoli gate can also be generated by a Rabi resonance method. It is a simple generalization of the CNOT gate. Indeed, it can be called a CNNOT gate in that two qubits need to be 1, to have a NOT gate act on the third qubit. The three qubit density matrix is in general:

$$\begin{aligned}
 \rho(t) &= \frac{1}{8}(\mathbf{1}_8 + \chi_A^P(t) + \chi_B^P(t) + \chi_C^P(t) + \chi_1^T(t) + \chi_2^T(t) + \chi_3^T(t) + \chi_4^T(t)) \\
 \chi_A^P(t) &= \sum_{i=1,3} P_i^A(t) \sigma_i^A \otimes \sigma_0^B \otimes \sigma_0^C \\
 \chi_B^P(t) &= \sum_{i=1,3} P_i^B(t) \sigma_0^A \otimes \sigma_i^B \otimes \sigma_0^C \\
 \chi_C^P(t) &= \sum_{i=1,3} P_i^C(t) \sigma_0^A \otimes \sigma_0^B \otimes \sigma_i^C \\
 \chi_1^T(t) &= \sum_{i,j=1,3} T_{ij}^{AB}(t) \sigma_i^A \otimes \sigma_j^B \otimes \sigma_0^C \\
 \chi_2^T(t) &= \sum_{i,j=1,3} T_{ij}^{AC}(t) \sigma_i^A \otimes \sigma_0^B \otimes \sigma_j^C \\
 \chi_3^T(t) &= \sum_{i,j=1,3} T_{ij}^{BC}(t) \sigma_0^A \otimes \sigma_i^B \otimes \sigma_j^C \\
 \chi_4^T(t) &= \sum_{i,j,k=1,3} T_{ijk}^{ABC}(t) \sigma_i^A \otimes \sigma_j^B \otimes \sigma_k^C.
 \end{aligned} \tag{C.1}$$

For three-qubits the density matrix has 63 real spin observables. The relations between the density matrix and the 63 spin observables are:

$$\begin{aligned}
 \vec{P}^A(t) &= \text{Tr}(\vec{\sigma}_A \otimes \sigma_0 \otimes \sigma_0) \rho(t) \equiv \langle \vec{\sigma}_A \otimes \sigma_0 \otimes \sigma_0 \rangle \\
 \vec{P}^B(t) &= \text{Tr}(\sigma_0 \otimes \vec{\sigma}_B \otimes \sigma_0) \rho(t) \equiv \langle \sigma_0 \otimes \vec{\sigma}_B \otimes \sigma_0 \rangle \\
 \vec{P}^C(t) &= \text{Tr}(\sigma_0 \otimes \sigma_0 \otimes \vec{\sigma}_C) \rho(t) \equiv \langle \sigma_0 \otimes \sigma_0 \otimes \vec{\sigma}_C \rangle \\
 \overleftrightarrow{T}_{AB}(t) &= \text{Tr}(\vec{\sigma}_A \otimes \vec{\sigma}_B \otimes \sigma_0) \rho(t) \equiv \langle \vec{\sigma}_A \otimes \vec{\sigma}_B \otimes \sigma_0 \rangle \\
 \overleftrightarrow{T}_{AC}(t) &= \text{Tr}(\vec{\sigma}_A \otimes \sigma_0 \otimes \vec{\sigma}_C) \rho(t) \equiv \langle \vec{\sigma}_A \otimes \sigma_0 \otimes \vec{\sigma}_C \rangle \\
 \overleftrightarrow{T}_{BC}(t) &= \text{Tr}(\sigma_0 \otimes \vec{\sigma}_B \otimes \vec{\sigma}_C) \rho(t) \equiv \langle \sigma_0 \otimes \vec{\sigma}_B \otimes \vec{\sigma}_C \rangle \\
 T_{ABC}(t) &\rightarrow \text{Tr}(\sigma_i \otimes \sigma_j \otimes \sigma_k) \rho(t) \equiv \langle \sigma_i \otimes \sigma_j \otimes \sigma_k \rangle.
 \end{aligned} \tag{C.2}$$

There are three polarizations $3 \times 3 = 9$, three double spin correlations $3 \times 9 = 27$, plus one triple spin correlation $3 \times 3 \times 3 = 27$, with a net of $9 + 27 + 27 = 63$ spin observables.

For the three qubit state $|q_1, q_2, q_3\rangle$ with q_1, q_2 as the control and q_3 as the action qubit we have the circuit TC=, with q_1, q_3 as the control and q_2 as the action qubit we have the circuit

TB=, and with q_2, q_3 as the control and q_1 as the action qubit we have the circuit TA=

. The corresponding matrices²⁵ are:

$$TC = \begin{pmatrix} 1 & 0 & 0 & 0 & 0 & 0 & 0 & 0 \\ 0 & 1 & 0 & 0 & 0 & 0 & 0 & 0 \\ 0 & 0 & 1 & 0 & 0 & 0 & 0 & 0 \\ 0 & 0 & 0 & 1 & 0 & 0 & 0 & 0 \\ 0 & 0 & 0 & 0 & 1 & 0 & 0 & 0 \\ 0 & 0 & 0 & 0 & 0 & 1 & 0 & 0 \\ 0 & 0 & 0 & 0 & 0 & 0 & 1 & 0 \\ 0 & 0 & 0 & 0 & 0 & 0 & 0 & 1 \end{pmatrix}. \tag{C.3}$$

$$TB = \begin{pmatrix} 1 & 0 & 0 & 0 & 0 & 0 & 0 & 0 \\ 0 & 1 & 0 & 0 & 0 & 0 & 0 & 0 \\ 0 & 0 & 1 & 0 & 0 & 0 & 0 & 0 \\ 0 & 0 & 0 & 1 & 0 & 0 & 0 & 0 \\ 0 & 0 & 0 & 0 & 1 & 0 & 0 & 0 \\ 0 & 0 & 0 & 0 & 0 & 1 & & 0 \\ 0 & 0 & 0 & 0 & 0 & 0 & 1 & 0 \\ 0 & 0 & 0 & 0 & 0 & 0 & 1 & 0 \end{pmatrix}. \tag{C.4}$$

$$TA = \begin{pmatrix} 1 & 0 & 0 & 0 & 0 & 0 & 0 & 0 \\ 0 & 1 & 0 & 0 & 0 & 0 & 0 & 0 \\ 0 & 0 & 1 & 0 & 0 & 0 & 0 & 0 \\ 0 & 0 & 0 & 0 & 0 & 0 & 0 & 1 \\ 0 & 0 & 0 & 0 & 1 & 0 & 0 & 0 \\ 0 & 0 & 0 & 0 & 0 & 1 & 0 & 0 \\ 0 & 0 & 0 & 0 & 0 & 0 & 1 & 0 \\ 0 & 0 & 0 & 1 & 0 & 0 & 0 & 0 \end{pmatrix}. \tag{C.5}$$

The main action of these Toffoli operators are that:

$$TC|1, 1, 1\rangle = |1, 1, 0\rangle \text{ and } TC|1, 1, 0\rangle = |1, 1, 1\rangle \tag{C.6}$$

$$TB|1, 1, 1\rangle = |1, 0, 1\rangle \text{ and } TB|1, 0, 1\rangle = |1, 1, 1\rangle \tag{C.7}$$

$$TA|0, 1, 1\rangle = |1, 1, 1\rangle \text{ and } TA|1, 1, 1\rangle = |0, 1, 1\rangle \tag{C.8}$$

For all other kets there are no qubit changes. How can this be implemented using the prior CNOT approach?

C.1. Hamiltonians

The main ingredients are again non-degenerate qubit levels, spin-spin interactions and Rabi driving fields along with appropriate choices of the resonant Rabi driving frequencies. The non-degenerate qubit levels are again produced by a constant magnetic field in the \hat{z} direction, with a

²⁵ These operators are defined by: $TC = I_8 + \mathcal{P}_1 \otimes \mathcal{P}_1 \otimes (\sigma_x - \sigma_0)$, $TB = I_8 + \mathcal{P}_1 \otimes (\sigma_x - \sigma_0) \otimes \mathcal{P}_1$, and $TA = I_8 + (\sigma_x - \sigma_0) \otimes \mathcal{P}_1 \otimes \mathcal{P}_1$, where \mathcal{P}_1 denotes a spin projection operator.

gradient in the qubit line-up \hat{x} direction, which yields a Hamiltonian

$$H_0 = -\frac{\omega_L^A}{2} \sigma_z \otimes \sigma_0 \otimes \sigma_0 - \frac{\omega_L^B}{2} \sigma_0 \otimes \sigma_z \otimes \sigma_0 - \frac{\omega_L^C}{2} \sigma_0 \otimes \sigma_0 \otimes \sigma_z, \tag{C.9}$$

for qubits A, B and C. We assume these frequencies are non-degenerate $\omega_L^A > \omega_L^B > \omega_L^C$. The spin-spin interactions acts between pairs of qubits:

$$\begin{aligned} V_{SS} &= \frac{J}{4} (\vec{\sigma}_A \cdot \vec{\sigma}_B - I_8) + \frac{J}{4} (\vec{\sigma}_A \cdot \vec{\sigma}_C - I_8) \\ &\quad + \frac{J}{4} (\vec{\sigma}_B \cdot \vec{\sigma}_C - I_8) \\ \vec{\sigma}^A \cdot \vec{\sigma}^B &\equiv \sum_{i=1,3} \vec{\sigma}_i \otimes \vec{\sigma}_i \otimes \sigma_0 \\ \vec{\sigma}^A \cdot \vec{\sigma}^C &\equiv \sum_{i=1,3} \vec{\sigma}_i \otimes \sigma_0 \otimes \vec{\sigma}_i \\ \vec{\sigma}^B \cdot \vec{\sigma}^C &\equiv \sum_{i=1,3} \sigma_0 \otimes \vec{\sigma}_i \otimes \vec{\sigma}_i \\ I_8 &\equiv \vec{\sigma}_0 \otimes \vec{\sigma}_0 \otimes \sigma_0 \end{aligned} \tag{C.10}$$

where we use a common strength J for each of the qubit pairs. It provides additional level splitting that allows for the controlled qubits to cause selective NOT gate action.

Finally, we have the Rabi term for each of the three qubits:

$$\begin{aligned} V_R(t) &= V_R^A(t) + V_R^B(t) + V_R^C(t) \\ V_R^A(t) &= \frac{\hbar\omega_2^R}{2} (\cos(\omega t) \sigma_x \otimes \sigma_0 \otimes \sigma_0 - \sin(\omega t) \sigma_y \otimes \sigma_0 \otimes \sigma_0) \\ V_R^B(t) &= \frac{\hbar\omega_2^R}{2} (\cos(\omega t) \sigma_0 \otimes \sigma_x \otimes \sigma_0 - \sin(\omega t) \sigma_0 \otimes \sigma_y \otimes \sigma_0) \\ V_R^C(t) &= \frac{\hbar\omega_2^R}{2} (\cos(\omega t) \sigma_0 \otimes \sigma_0 \otimes \sigma_x - \sin(\omega t) \sigma_0 \otimes \sigma_0 \otimes \sigma_y) \end{aligned} \tag{C.11}$$

Here $\omega_2^R = \omega_2$ specifies the common strength of the three driving terms and ω denotes the common Rabi driving frequency. It is the choice of a resonant value for ω along with the spin-spin interaction and non-degeneracy that produces the control(s) and action dynamics.²⁶

C.2. First rotating frame

As before we first transform to the first rotating frame using the following unitary matrices for qubits A, B and C with the same driving frequency $U_1(t) \equiv e^{+\frac{i}{2}\omega\sigma_z^A t} \otimes e^{+\frac{i}{2}\omega\sigma_z^B t} \otimes e^{+\frac{i}{2}\omega\sigma_z^C t}$, We again use the rule in Eq. (A.1). The spin-spin term V_{SS} is unchanged. The $H_0 + V^R(t)$ transforms to $H_{20} + V_2^R(t)$ in the first rotated frame

$$H_{20} = \hbar\left\{ \frac{\omega - \omega_L^A}{2} \sigma_z \otimes \sigma_0 \otimes \sigma_0 + \frac{\omega - \omega_L^B}{2} \sigma_0 \otimes \sigma_z \otimes \sigma_0 + \frac{\omega - \omega_L^C}{2} \sigma_0 \otimes \sigma_0 \otimes \sigma_z \right\}, \tag{C.12}$$

for qubits A, B and C.

$$V_2^R = \frac{\hbar\omega_2^R}{2} (\sigma_x \otimes \sigma_0 \otimes \sigma_0 + \sigma_0 \otimes \sigma_x \otimes \sigma_0 + \sigma_0 \otimes \sigma_0 \otimes \sigma_x) \tag{C.13}$$

Note that in the first rotation frame $H_{20} + V_2^R + V_{SS}$ is time independent.

²⁶ The above case involves the NOT gate, although other choices could be made to generate controlled-any operator cases.

C.3. Resonant Rabi frequency

Three Rabi resonant frequencies produce three different Toffoli operators TA, TB, TC . The Rabi resonant frequencies are determined by the Hamiltonian $H_{20} + V_{SS}$. Based on a perturbation evaluation of $\det(H_{20} + V_{SS} - \omega) \equiv 0$, the associated transition Rabi frequencies are:

$$\text{For TC : } \delta_{110}^{111} = \omega_C^L + J - \frac{J^2}{4} \left(\frac{1}{\Delta_1} + \frac{1}{\Delta_2} \right) - \frac{J^3}{4\Delta_1\Delta_2}.$$

$$\text{For TB : } \delta_{101}^{111} = \omega_B^L + J - \frac{J^2}{4} \left(\frac{1}{\Delta} - \frac{1}{\Delta_2} \right) + \frac{J^3}{4\Delta\Delta_2}.$$

$$\text{For TA : } \delta_{011}^{111} = \omega_A^L + J + \frac{J^2}{4} \left(\frac{1}{\Delta} + \frac{1}{\Delta_1} \right) - \frac{J^3}{4\Delta\Delta_1},$$

with $\Delta \equiv \omega_L^A - \omega_L^B$, $\Delta_1 \equiv \omega_L^A - \omega_L^C$, and $\Delta_2 \equiv \omega_L^B - \omega_L^C$. Selection of $w = \delta_{110}^{111}, \delta_{101}^{111}$ or δ_{011}^{111} , along with a numerical solution of the time-dependent density matrix generates the associated Toffoli gate.

C.4. Numerical Toffoli gates

For example, assume an initial density matrix $\rho(0) = |110\rangle\langle 110|$, and taking Rabi driving resonance frequency $\omega = \delta_{110}^{111}$. The analytic method yields the final density matrix $\rho(t_f) = TC.\rho(0).TC$. The exact initial nonzero spin observables are: $P_z^A = P_z^B = 1 = -P_z^C, T_{zz}^{AB} = -T_{zz}^{AC} = -T_{zz}^{BC} = 1 = T_{zz}^{ABC}$. The exact final nonzero spin observables are: $P_z^A = P_z^B = 1 = P_z^C, T_{zz}^{AB} = T_{zz}^{AC} = T_{zz}^{BC} = 1 = -T_{zz}^{ABC}$. Now calculate the dynamical density matrix numerically. Numerical solution for the three-qubit first rotation frame density matrix with three Rabi driving resonance frequencies ω are shown in Fig. C.20.

Appendix D. Noise and Lindblad

D.1. Lindblad noise pulses- L_N

The Lindblad term \mathcal{L}_1 is adopted as a mechanism for introducing external noise effects. When so used we denote the associated Lindblad operator as $L(t) \rightarrow L_N(t)$, where we focus on weak single qubit and distinct pulses of short duration. In that case a single time-dependent $L_N(t)$ suffices for our present study. For example, we define $L_N^a(t)$ for qubit A as

$$L_N^a(t) = \sigma_0 + \sum_{\mu} \eta_{\mu} \vec{\sigma} \cdot \hat{n}_{\mu} \phi(t - t_{\mu}), \tag{D.1}$$

where $\hat{n}_{\mu} \equiv \{\sin \theta_{\mu} \cos \phi_{\mu}, \sin \theta_{\mu} \sin \phi_{\mu}, \cos \theta_{\mu}\}$ for random values of $0 \leq \theta_{\mu} \leq \pi$, and $0 \leq \phi_{\mu} \leq 2\pi$ and for random lengths $\eta_{\mu} \leq 1$, and random times t_{μ} , for each integer value of $\mu = 1 \dots n_h$.²⁷ The total number of noise hits on that qubit is n_h , where overlapping hits are removed. That is what is meant by distinct hits. The above steps are also applied to qubit B and the resultant Lindblad two-qubit noise operator is $L_N(t) = L_N^a(t) \otimes L_N^b(t)$. The random time for each noise hit t_{μ} is often restricted to the time region that a gate is in action to examine the stability of a particular gate. The strength of a particular hit is $\Gamma \eta_{\mu}$, which is limited to small amplitudes. A typical set of such noise hits is Fig. D.21.

²⁷ See [8] for how to assure uniform distribution of points within the Bloch ball.

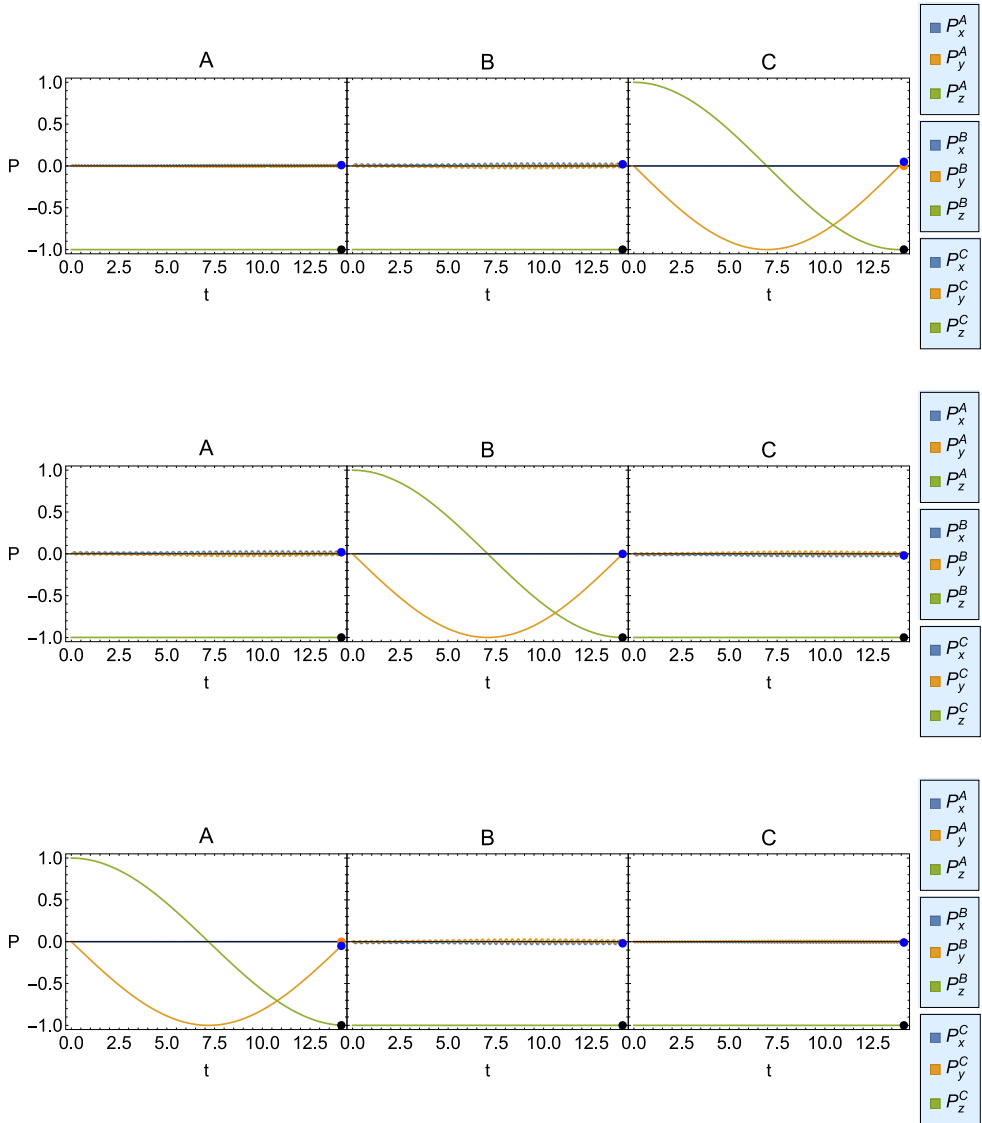


Fig. C.20. Toffoli gate T: (top) TC with initial qubits = $|110\rangle$ and $\omega = \delta_{110}^{111}$; (center) TB with initial qubits = $|101\rangle$ and $\omega = \delta_{101}^{111}$; (bottom) TA with initial qubits = $|011\rangle$ and $\omega = \delta_{011}^{111}$. The density matrix is solved numerically with typical Table 2 values. Precision of this calculation is $\text{Tr}(\rho(t_f) \cdot T \cdot \rho(t_i) \cdot T) \cong 99.99\%$. The other 54 observables are quite precise as indicated by a Hilbert–Schmidt distance study.

D.2. \mathcal{L}_{NC} noise compensation with purity increase and associated entropy decrease

The condition for selecting Lindblad noise that decreases purity and consequently increases entropy is given in Eq. (63). Let us examine this for a single qubit. Here we use $\mathcal{L}_1 \rightarrow \mathcal{L}_N$ for noise and in addition $\mathcal{L}_1 \rightarrow \mathcal{L}_{NC}$ for noise compensation.

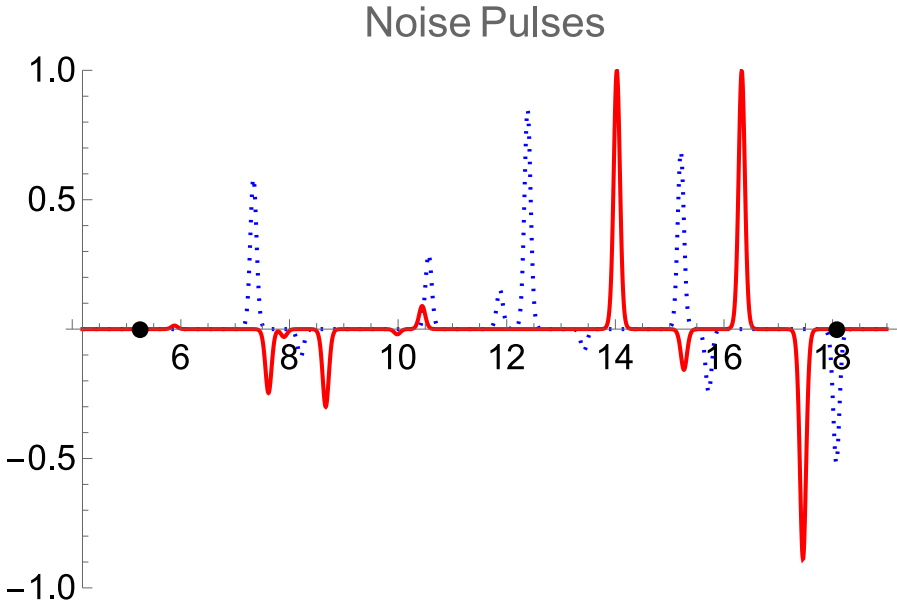


Fig. D.21. Noise pulses on two qubits for 12 hits, with overlaps dropped for each qubit. The solid red curves are for qubit A and the dotted blue are for qubit B. The pulses have common widths of 0.2, with random strengths. The black dots indicate the on/off times of the CNOT gate pulse; so this generates external Lindblad noise during that gate.

The Lindblad operator is expanded as $L(t) = \sum_{i=0,3} \mathbb{L}_i \sigma_i$, then $L^\dagger(t) = \sum_{i=0,3} \mathbb{L}_i^* \sigma_i$. The $i = 0$ terms do not contribute and we obtain the contribution of \mathcal{L}_{NC} to the rate of change of purity $\mathcal{P}(t)$ as

$$\begin{aligned} \dot{\mathcal{P}}(t) &= 2 \operatorname{Tr}(\rho \mathcal{L}_{NC}) \\ \dot{\mathcal{P}}(t) &= \sum_{i,j=1,3} \mathbb{L}_i^* \mathbb{M}_{i,j} \mathbb{L}_j \\ \mathbb{M}_{i,j} &= 2 \gamma_{NC} \operatorname{Tr}(\rho \sigma_j \rho \sigma_i - \frac{1}{2}(\rho \rho + \rho \rho) \sigma_i \sigma_j). \end{aligned} \tag{D.2}$$

Here ρ is a dynamically calculated density matrix at a selected time, whereas ρ is a guessed density matrix used to specify \mathcal{L}_{NC} , see later. Let us equate these for now. Then with γ_{NC} set to one,

$$\mathbb{M}_{i,j} = 2 \operatorname{Tr}(\rho \sigma_j \rho \sigma_i - \rho \rho \sigma_i \sigma_j) \tag{D.3}$$

where $\mathbb{M} = \mathbb{M}_R + i \mathbb{M}_I$ is now a 3×3 Hermitian matrix with trace -2 and zero determinant. Thus the three eigenvalues are real, with one zero and the others two sum to $-4 P^2$.

$$\mathbb{M}_R = 2 P^2 \begin{pmatrix} -\sin^2(\theta) \sin^2(\phi) - \cos^2(\theta) & \sin^2(\theta) \sin(\phi) \cos(\phi) & \sin(\theta) \cos(\theta) \cos(\phi) \\ \sin^2(\theta) \sin(\phi) \cos(\phi) & -\sin^2(\theta) \cos^2(\phi) - \cos^2(\theta) & \sin(\theta) \cos(\theta) \sin(\phi) \\ \sin(\theta) \cos(\theta) \cos(\phi) & \sin(\theta) \cos(\theta) \sin(\phi) & -\sin^2(\theta) \end{pmatrix} \tag{D.4}$$

$$\mathbb{M}_I = 2 P \begin{pmatrix} 0 & \cos(\theta) & -\sin(\theta) \sin(\phi) \\ -\cos(\theta) & 0 & \sin(\theta) \cos(\phi) \\ \sin(\theta) \sin(\phi) & -\sin(\theta) \cos(\phi) & 0 \end{pmatrix}. \tag{D.5}$$

The three eigenvalues of \mathbb{M} are $\lambda_0 = 0, \lambda_+ = +2P(1 - P), \lambda_- = -2P(1 + P)$, where $P \leq 1$ is the magnitude of the inside the Bloch ball polarization vector. The normalized eigenvectors for these three eigenvalues are:

$$\begin{aligned} \vec{V}_0(\theta, \phi) &= \hat{n}_P = \frac{\vec{P}}{P} = \{\sin \theta \cos \phi, \sin \theta \sin \phi, \cos \theta\} \\ \vec{V}_+ &= \frac{1}{\sqrt{2}}\{-\cos \theta \cos \phi - i \sin \phi, -\cos \theta \sin \phi + i \cos \phi, \sin \theta\} \\ &= \vec{V}_R + i \vec{V}_I \\ \vec{V}_- &= \frac{1}{\sqrt{2}}\{-\cos \theta \cos \phi + i \sin \phi, -\cos \theta \sin \phi - i \cos \phi, \sin \theta\} \\ &= \vec{V}_R - i \vec{V}_I \end{aligned} \tag{D.6}$$

$$\begin{aligned} \vec{V}_R &= \frac{1}{\sqrt{2}}\{-\cos \theta \cos \phi, -\cos \theta \sin \phi, \sin \theta\} = \frac{1}{\sqrt{2}}\vec{V}_0(\theta - \frac{\pi}{2}, \phi) \\ \vec{V}_I &= \frac{1}{\sqrt{2}}\{-\sin \phi, +\cos \phi, 0\} = \frac{1}{\sqrt{2}}\vec{V}_0(-\frac{\pi}{2}, \phi - \frac{\pi}{2}), \end{aligned} \tag{D.7}$$

where $P = \sqrt{P_x^2 + P_y^2 + P_z^2}$ is the magnitude of the polarization vector with components $\vec{P} = \{P_x, P_y, P_z\}$ for a single qubit density matrix ρ . We see above that the eigenvectors with nonzero eigenvalues are related to the zero eigenvalue case by simple rotations.

Now selecting \vec{V}_+ will produce increased purity and lower entropy. If we identify the eigenvectors of \mathbb{M} as $\{\vec{V}_0, \vec{V}_+, \vec{V}_-\} \rightarrow \{\mathbb{L}_1, \mathbb{L}_2, \mathbb{L}_3\}$, we can associate the positive eigenvalue with increasing purity and the negative eigenvalue with decreasing purity. The zero eigenvalue part yields no change in purity. The usual constraint is to have Lindblad operators that decrease Purity and thus increase entropy. Here to use this structure for noise control (NC), we select Lindblad operators with the above positive eigenvalue of \mathbb{M} , which yields increased purity and decreased entropy. That step reverses the increase in entropy associated with noise. It also means that we violate the condition given in Eq. (64) and now can invoke non-Hermitian Lindblad operators as a noise control mechanism.

In the above discussion, we identify the eigenvectors of \mathbb{M} as a way to define three types of Lindblad operators; one that does not change purity \mathbb{L}_1 , one that increases purity \mathbb{L}_2 and one that decreases purity \mathbb{L}_3 . The density matrix used to define \mathbb{M} and the associated polarization vector $\vec{P} : \{P_x, P_y, P_z\}$ in general differs from the polarization vector $\vec{P} : \{\mathbf{P}_x, \mathbf{P}_y, \mathbf{P}_z\}$ associated with a qubit's dynamically calculated values, including possible noise effects. In a real case one calculates \vec{P} from the dynamic equations and guesses \vec{P} based on values that one would like to realize at a particular time, such as towards the end times of a gate. The role of \vec{P} , and \vec{P} in influencing changes in purity²⁸ is given by $\delta\dot{\mathcal{P}}(t) = 2 \text{Tr}(\rho \mathcal{L}_1)$, where ρ is based on the dynamic \vec{P} and \mathcal{L}_1 uses the best guess values \vec{P}

$$\begin{aligned} \mathbb{L}_1 : \delta\dot{\mathcal{P}}(t) &= 0 \\ \mathbb{L}_2 : \delta\dot{\mathcal{P}}(t) &= +\frac{2(1 - P)}{P} (\vec{P} \cdot \vec{P}) \\ \mathbb{L}_3 : \delta\dot{\mathcal{P}}(t) &= -\frac{2(1 + P)}{P} (\vec{P} \cdot \vec{P}). \end{aligned} \tag{D.8}$$

In the $\vec{P} \rightarrow \vec{P}$ limit this reduces to the earlier result. Note the middle case above is the key one with an increase in Purity provided $\vec{P} \cdot \vec{P}$ is positive. A good guess must satisfy that condition if a decrease in entropy is needed to control noise.

²⁸ Our focus in these sections is on the contribution from the \mathcal{L}_1 , which must be added to that from other \mathcal{L} terms.

An additional insight into the role of the Lindblad operator L in \mathcal{L}_1 is seen by the effect on the one-qubit polarization:

$$\begin{aligned}
 \mathbb{L}_1 : \delta \vec{P}(t) &= -2\vec{P} + 2 \frac{\vec{P} \cdot \vec{P}}{\mathbf{P}} \frac{\vec{P}}{\mathbf{P}} \xrightarrow{\vec{P} \rightarrow \vec{P}} 0 \\
 \mathbb{L}_2 : \delta \vec{P}(t) &= -\vec{P} + (2 - \frac{\vec{P} \cdot \vec{P}}{\mathbf{P}}) \frac{\vec{P}}{\mathbf{P}} \xrightarrow{\vec{P} \rightarrow \vec{P}} 2 \frac{1-P}{P} \vec{P} \\
 \mathbb{L}_3 : \delta \vec{P}(t) &= -\vec{P} - (2 + \frac{\vec{P} \cdot \vec{P}}{\mathbf{P}}) \frac{\vec{P}}{\mathbf{P}} \xrightarrow{\vec{P} \rightarrow \vec{P}} -2 \frac{1+P}{P} \vec{P}
 \end{aligned} \tag{D.9}$$

Limits for the three Lindblad cases are shown. From these results, it follows that entropy decreases and the associated eigenvalues are pushed closer together for \mathbb{L}_2 . It can be shown that the Lidar condition (64) can be broken using the Lindblad operator \mathbb{L}_2 , which is also non-Hermitian.

Evaluating \mathcal{L}_1 for each of the above \mathbb{L}_i cases yields a simple result:

$$\begin{aligned}
 \mathcal{L}_1(\mathbb{L}_1) &= -\left[\vec{P} - (\vec{P} \cdot \hat{\mathbf{n}}_{\mathbf{P}}) \hat{\mathbf{n}}_{\mathbf{P}}\right] \cdot \vec{\sigma} \xrightarrow{\vec{P} \rightarrow \vec{P}} 0 \\
 \mathcal{L}_1(\mathbb{L}_2) &= -\frac{1}{2} \left[\vec{P} - (2 - \vec{P} \cdot \hat{\mathbf{n}}_{\mathbf{P}}) \hat{\mathbf{n}}_{\mathbf{P}}\right] \cdot \vec{\sigma} \xrightarrow{\vec{P} \rightarrow \vec{P}} \frac{1-P}{P} (\vec{\sigma} \cdot \vec{P}) \\
 \mathcal{L}_1(\mathbb{L}_3) &= -\frac{1}{2} \left[\vec{P} + (2 + \vec{P} \cdot \hat{\mathbf{n}}_{\mathbf{P}}) \hat{\mathbf{n}}_{\mathbf{P}}\right] \cdot \vec{\sigma} \xrightarrow{\vec{P} \rightarrow \vec{P}} -\frac{1+P}{P} (\vec{\sigma} \cdot \vec{P})
 \end{aligned} \tag{D.10}$$

where $\hat{\mathbf{n}}_{\mathbf{P}} \equiv \frac{\vec{P}}{P}$. This result can be used to recover the Purity, polarization and entropy rates contributions from \mathcal{L}_1 .

The above one-qubit case discussion to two or more qubits. For the two qubit case the \mathbb{M} is a 16×16 Hermitian matrix with 6 positive, 6 negative and 4 zero eigenvalues. The largest of the positive eigenvalues and its associated eigenvector would be the most effective choice for an entropy reduction for two-qubit Lindblad noise pulses. Double noise hits are less likely and hence we do not pursue such cases here, but simply apply single-qubit NC Lindblad pulses on each qubit.

D.3. LNC simple noise compensation via decrease in entropy

The above analysis allows one to select a Lindblad operator that perform increases purity and decreases entropy. That is an operator that restores order in some sense. Ideally, one could use sophisticated, albeit costly, error correction methods to optimally design such a Lindblad entropy decreasing operator. As a simple alternative, one could assume that the barrage of noise would bend towards increasing entropy and use an entropy reduction series of Lindblad pulses to counter the effect of noise. The advantage of this uninformed step is that one need not invoke the heavy costs of error correction; the disadvantage is that it is a gamble without assurance of success. Nevertheless if one knows from model calculations where the system should be, that could affect the design of the noise canceling steps (NC). This scheme is explored in the main text, where it is indeed seen to cancel noise.

Appendix E. Noise compensation Lindblad in Hamiltonian form

To gain insight on how to implement noise compensation via selection of a Lindblad that increases purity and decreases entropy, it is helpful to cast \mathcal{L}_{NC} into Hamiltonian form. We would like to find some approximate Hamiltonian $H_{\eta}(t)$, albeit non-hermitian, that allows the substitution $\mathcal{L}_{NC}(t) \rightarrow i[\rho(t), H_{\eta}(t)]$. We can see if the associated condition

$$i \text{Tr}(\Omega^{\kappa} [\rho(t), H_{\eta}(t)]) \leftrightarrow \text{Tr}(\Omega^{\kappa} \mathcal{L}_{NC})$$

can be satisfied. Here Ω^{κ} denotes the full set of spin operators for n_q qubits. For example, for one qubit $\Omega = \vec{\sigma}$. In general the above condition cannot be satisfied.

However, one direct way to find an approximate solution is to invoke the pseudoinverse (Moore-Penrose inverse) of the commutator term. For example, for one qubit use $H_{\eta}(t) = \vec{\sigma} \cdot \vec{h}_{\eta}(t)$ to find an

approximate solution for \bar{h}_η . That was carried out numerically for one and two qubits and the result is a non-hermitian Hamiltonian. The task then is to generate such a Hamiltonian using absorptive magnetic and possibly electric field pulses. That task is relegated to a future study.

References

- [1] Frank Tabakin, *Ann. Physics* 383 (2017) 33–78.
- [2] Andrzej Kossakowski, *Rep. Math. Phys.* 3 (4) (1972) 247–274.
- [3] Goran Lindblad, *Comm. Math. Phys.* 48 (1976) 119–130.
- [4] Vittorio Gorini, Andrzej Kossakowski, Ennackal Chandu George Sudarshan, *J. Math. Phys.* 17 (5) (1976) 821–825.
- [5] C. Lindblad, *Non-Equilibrium Entropy and Irreversibility*, Vol. 5, Springer Science & Business Media, 2001.
- [6] Gian Paolo Beretta, *Phil. Trans. R. Soc. A* 378 (2170) (2020) 20190168.
- [7] G.P. Beretta, Omar Al-Abbasi, M.R. von Spakovsky, *Phys. Rev. E* 95 (4) (2017) 042139.
- [8] Sergio Cano-Andrade, Gian Paolo Beretta, Michael R. von Spakovsky, *Phys. Rev. A* 91 (1) (2015) 013848.
- [9] Gian Paolo Beretta, *J. Phys. Conf. Ser.* 237 (1) (2010) 012004.
- [10] Gian Paolo Beretta, *Rep. Math. Phys.* 64 (1–2) (2009) 139–168.
- [11] Gian Paolo Beretta, *Int. J. Quantum Inf.* 05 (01n02) (2007) 249–255.
- [12] Gian Paolo Beretta, *Modern Phys. Lett. A* 20 (13) (2005) 977–984.
- [13] G.P. Beretta, E.P. Gyftopoulos, J.L. Park, *Nuovo Cimento B* 87 (1985) 77–97.
- [14] G.P. Beretta, E.P. Gyftopoulos, J.L. Park, G.N. Hatsopoulos, *Nuovo Cimento B* (1984) 169–191.
- [15] George N. Hatsopoulos, Elias P. Gyftopoulos, *Found. Phys.* 6 (2) (1976) 127–141.
- [16] Clemens Müller, Thomas M. Stace, *Phys. Rev. A* 95 (1) (2017) 013847.
- [17] Leonid V. Keldysh, et al., *Sov. Phys.—JETP* 20 (4) (1965) 1018–1026.
- [18] John von Neumann, *Mathematical Foundations of Quantum Mechanics*, Princeton University Press. Springer-Verlag, 2018.
- [19] Lev Landau, *Z. Phys.* 45 (5) (1927) 430–441.
- [20] Ugo Fano, *Rev. Modern Phys.* 29 (1) (1957) 74.
- [21] J.A. Montañez-Barrera, R.T. Holladay, G.P. Beretta, Michael R. von Spakovsky, *Quantum Inf. Process.* 21 (9) (2022) 314.
- [22] Maciej Kuna, Jan Naudts, *Rep. Math. Phys.* 65 (1) (2010) 77–108.
- [23] Maximilian Russ, Guido Burkard, *J. Phys.: Condens. Matter* 29 (39) (2017) 393001.
- [24] Maximilian Russ, David M. Zajac, Anthony J. Sigillito, Felix Borjans, Jacob M. Taylor, Jason R. Petta, Guido Burkard, *Phys. Rev. B* 97 (8) (2018) 085421.
- [25] Luca Petit, Maximilian Russ, Gertjan H.G.J. Eenink, William I.L. Lawrie, James S. Clarke, Lieven M.K. Vandersypen, Menno Veldhorst, *Commun. Mater.* 3 (1) (2022) 1–7.
- [26] Thaddeus D. Ladd, Malcolm S. Carroll, *Encyclopedia of Modern Optics*, Vol. 1, 2018, pp. 467–477.
- [27] Rohit Kishan Ray, Gian Paolo Beretta, 2023, arXiv:2301.11548 [quant-ph].
- [28] Alfréd Rényi, *Proceedings of the Fourth Berkeley Symposium on Mathematical Statistics and Probability*, Volume 1: Contributions to the Theory of Statistics, Vol. 4, University of California Press, 1961, pp. 547–562.
- [29] J. Balatoni, A. Rényi, *Publ. Math. Inst. Hung. Acad. Sci.* 1 (1956) 9–40.
- [30] Alfréd Rényi, *Selected Papers of Alfréd Rényi*, Vol. 1, Akadémiai Kiadó, 1976.
- [31] D.A. Lidar, A. Shabani, R. Alicki, *Chem. Phys.* 322 (1–2) (2006) 82–86.
- [32] Daniel Manzano, *AIP Adv.* 10 (2) (2014) 025106.
- [33] Norman F. Ramsey, *Phys. Rev.* 103 (1) (1956) 20.
- [34] Simon Braun, Jens Philipp Ronzheimer, Michael Schreiber, Sean S. Hodgman, Tim Rom, Immanuel Bloch, Ulrich Schneider, *Science* 339 (6115) (2013) 52–55.
- [35] Daan Frenkel, Patrick B. Warren, *Amer. J. Phys.* 83 (2) (2015) 163–170.
- [36] Bruno Juliá-Díaz, Joseph M. Burdiss, Frank Tabakin, *Comput. Phys. Comm.* 180 (3) (2009) 474.
- [37] Frank Tabakin, Bruno Juliá-Díaz, *Comput. Phys. Comm.* 182 (8) (2011) 1693–1707.
- [38] Frank Tabakin, *Wolfram Community* (2022).
- [39] Carole Addis, Elsi-Mari Laine, Clemens Gneiting, Sabrina Maniscalco, *Phys. Rev. A* 94 (5) (2016) 052117.
- [40] Rohit Kishan Ray, *Phys. Rev. E* 106 (2) (2022) 024115.
- [41] Tenpei Morishita, Kiyoshi Kobayashi, Akira Ishikawa, *J. Phys. Soc. Japan* 92 (2) (2023) 024001.
- [42] J.A. Montanez-Barrera, Cesar E. Damian-Ascencio, Michael R. von Spakovsky, Sergio Cano-Andrade, *Phys. Rev. A* 101 (5) (2020) 052336.
- [43] Yu. I. Bogdanov, A. Yu. Chernyavskiy, Alexander Holevo, V.F. Lukichev, A.A. Orlikovsky, *International Conference Micro-and Nano-Electronics 2012*, Vol. 8700, SPIE, 2013, pp. 404–415.
- [44] Irina Heinz, Guido Burkard, *Phys. Rev. B* 105 (12) (2022) L121402.
- [45] Stephan G.J. Philips, Mateusz T. Maździak, Sergey V. Amitonov, Sander L. de Snoo, Maximilian Russ, Nima Kalhor, Christian Volk, William I.L. Lawrie, Delphine Brousse, Larisa Trypuzen, et al., *Nature* 609 (7929) (2022) 919–924.
- [46] Benedikt Tissot, Michael Trupke, Philipp Koller, Thomas Astner, Guido Burkard, *Phys. Rev. Res.* 4 (3) (2022) 033107.
- [47] Piotr Szańkowski, Marek Trippenbach, Łukasz Cywiński, Yehuda B. Band, *Quantum Inf. Process.* 14 (2015) 3367–3397.
- [48] Rohit Kishan Ray, *Finite-Dimensional Quantum Systems under the Fourth Law of Thermodynamics* (Ph. D.), Indian Institute of Technology Kharagpur, Department of Physics Indian Institute of Technology, Kharagpur, 2023.
- [49] Isidor Isaac Rabi, N.F. Ramsey, *J. Schwinger, Rev. Modern Phys.* 26 (2) (1954) 167.
- [50] Katharina Kormann, Sverker Holmgren, Hans O. Karlsson, *J. Chem. Phys.* 128 (18) (2008) 184101.